High Energy Density Systems in Cryogenic Media: The Production and Reactions of Atoms and Radicals

Eric Weitz

Northwestern University
Department of Chemistry
2145 Sheridan Road
Evanston IL 60208−3113

DTIC
ELECTE
JAN 1 8 1995
S
G
D

November 1994

Final Report

19950117 035

DTIC QUALITY INSPECTED 3

PHILLIPS LABORATORY
Propulsion Directorate
AIR FORCE MATERIEL COMMAND
EDWARDS AIR FORCE BASE CA 93524−7001

NOTICE

When U.S. Government drawings, specifications, or other data are used for any purpose other than a definitely related Government procurement operation, the fact that the Government may have formulated, furnished, or in any way supplied the said drawings, specifications, or other data, is not to be regarded by implication or otherwise, or in any way licensing the holder or any other person or corporation, or conveying any rights or permission to manufacture, use or sell any patented invention that may be related thereto.
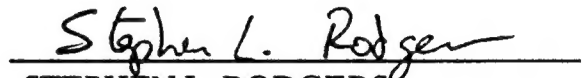
FOREWORD

This final technical report was prepared by Northwestern University, Evanston IL, under contract F04611−91−C−0016, for Operating Location AC, Phillips Laboratory, Edwards AFB CA 93524−7001. Project Manager for Phillips Laboratory was Michelle DeRose.
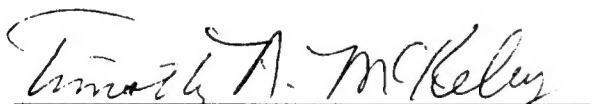
The report has been reviewed and is approved for release and distribution in accordance with the distribution statement on the cover and on the SF Form 298.
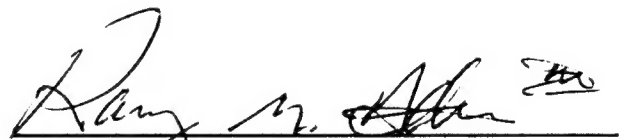

MICHELLE E. DEROSE
Project Manager

STEPHEN L. RODGERS
Chief, Emerging Technologies Branch

TIMOTHY A. MCKELVEY, Maj, USAF
Acting Director
Fundamental Technologies Division

RANNEY G. ADAMS, III
Public Affairs Director

REPORT DOCUMENTATION PAGE

Public reporting burden for this collection of information is estimated to average 1 hour per responce, including the time for reviewing instructions searching existing data sources gathering and maintaining the data needed, and completing and reviewing the collection of information. Send comments regarding this burden estimate or any other aspect of this collection of information, including suggestions for reducing this burden to Washington Headquarters Services, Directorate for Information Operations and Reports, 1215 Jefferson Davis Highway, Suite 1204, Arlington, VA 22202-4302, and to the Office of Management and Budget, Paperwork Reduction Project (0740-0188), Washington DC 20503,

1. AGENCY USE ONLY (LEAVE BLANK)	2. REPORT DATE November 1994	3. REPORT TYPE AND DATES COVERED Final 21 May 90 – 1 Oct 94

4. TITLE AND SUBTITLE

High Energy Density Systems in Cryogenic Media: The Production and Reactions of Atoms and Radicals

6. AUTHOR(S)

Eric Weitz

5. FUNDING NUMBERS

C: F29601-91-C-0016

PE: 62302F

PR: 5730

TA: 00BW

7. PERFORMING ORGANIZATION NAME(S) AND ADDRESS(ES)

Northwestern University
Department of Chemistry
2145 Sheridan Road
Evanston IL 60208-3113

8. PERFORMING ORGANIZATION REPORT NUMBER

9. SPONSORING/MONITORING AGENCY NAME(S) AND ADDRESS(ES)

Phillips Laboratory
OLAC PL/RKFE
9 Antares Road
Edwards AFB CA 93523-7680

10. SPONSORING/MONITORING AGENCY REPORT NUMBER

PL-TR-94-3050

11. SUPPLEMENTARY NOTES

COSATI CODE(S): 2005; 0705; 2013

12a. DISTRIBUTION/AVAILABILITY STATEMENT

Approved for Publiv Release; Distribution is Unlimited

12b. DISTRIBUTION CODE

13. ABSTRACT (MAXIMUM 200 WORDS)

The work in this study has been directed towards developing an understanding of the factors that affect the production and storage of energetic species in a cryogenic environment and to evaluate the feasibility of employing such a medium for use as a high energy density material. Matrix isolation techniques have been employed to produce and attempt to store reactive species, specifically atoms in cryogenic solids, with a focus on storage of O and H atoms. Factors that must be considered in optimizing the storage of photolytically produced atoms include: matrix temperature, photolysis wavelength, spin state of the atoms, reactions with co-fragments and parent, the relative mass of the photofragments, and diffusion and photoinduced diffusion of the photofragments and/or the parent molecule. The interplay between these factors and their effect on atom storage is considered. O atom storage in solid Xe at a 32 mmolar concentration has been achieved with a number of enumerated strategies possible for increasing this concentration. H atoms have been successfully isolated and are stable in solid Xe for days at a temperature of 10 K. Progress directed towards storing O atoms in solid O_2 is reported on.

14. SUBJECT TERMS
atoms; cryogenic; photolytic; radicals

15. NUMBER OF PAGES
44

16. PRICE CODE

17. SECURITY CLASSIFICATION OF REPORT	18. SECURITY CLASSIFICATION OF THIS PAGE	19. SECURITY CLASSIFICATION OF ABSTRACT	20. LIMITATION OF ABSTRACT
Unclassified	Unclassified	Unclassified	SAR

Table of Contents

List of Figures

List of Tables

INTRODUCTION

Contract F29609-91-C-0016 was directed towards developing an understanding of the factors that effect the production and storage of energetic species in a cryogenic environment and to evaluate the feasibility of such a medium for use as a high energy density material. Our approach involved using well tested matrix isolation techniques to produce and attempt to store reactive species: specifically atoms in this environment. We focused on developing an understanding of the factors that control the production and loss of these species as well as the factors that limit the storable concentration of reactive species. Four papers that acknowledge support from this contract have been published,[1-4] one is in press[5] and three more are in preparation.[6-8] Additional publications are likely in the future.

Before matrices can be optimized as vehicles for the storage of chemical energy, a number of fundamental issues regarding matrix photochemistry and matrix atom and radical chemistry must be addressed. Specific issues include:

1) How easily can radicals or atoms be photochemically generated in matrices? A related issue is how the matrix environment influences branching ratios for photochemistry and the "cage" effect.

2) How does the matrix environment influence the rates of chemical reactions versus the gas phase? In matrices, species must diffuse through the host to get to reactants. Will matrix reactions of radicals and/or atoms be diffusion limited? What are the magnitudes of diffusion coefficients for atoms and reactive radicals? How are these diffusion coefficients effected by the nature of the matrix and its temperature?

3) How does the lower temperature of the matrix environment influence chemistry? Are gas phase activation energies suitable for matrix reactions at much lower temperatures? Does tunneling become an important channel for these reactions at low temperature?

4) From the point of view of energy storage, it is important to investigate the concentration of atoms or radicals that can be "stored" in a matrix. Obviously this concentration will depend on the atom or radical, the matrix material, the temperature and the parent that is used to produce the reactive species.

The studies we have undertaken have attempted to address many of these questions. Traditionally, matrix isolation studies have focused on obtaining spectroscopic information about reactive and/or transient species.[9] Though still limited in both number and scope many of the more recent studies that have been directed towards elucidating the dynamics of matrix isolated species have yielded very interesting results.[10-13] The issue of molecular and atomic mobility and the reactions that can occur as a result of this mobility has been treated more extensively in disordered glasses[14] but has recently received some attention in condensed phase rare gases. We address this issue for both O atoms and H atoms in rare gas solids. Both thermal and photoinduced mobilities have been considered.[1-7,15-18] The latter process can occur as a result of dissociative relaxation of an exciplex which results in the constituent atoms being placed on a repulsive ground state potential energy surface. Under these circumstances a preponderance of the excess energy is disposed in the translational degrees of freedom of the light atom. For O atoms in xenon matrices this can result in O atom motion of potentially hundreds of angstroms.[2] We have investigated the dynamics of this process in detail. We have also considered the factors that limit O atom production in cryogenic environments and have shown that it is possible to store chemically

1

significant quantities of O atoms in such an environment. Preliminary work has also been performed on the storage of O atoms in solid O_2.

In this system $O(^1D)$ atoms are produced as a result of 193 nm photolysis of N_2O.[19] We have shown that reactions of $O(^1D)$ can be an important factor in limiting the concentration of stored O atoms. We have also demonstrated that in cage recombination can occur between N_2 and $O(^1D)$ and that this process is matrix morphology dependant. The photodissociation cross-section for N_2O is also shown to be morphology dependant.[5]

Though extensive studies of H atom mobilities and reaction kinetics have been undertaken in disordered organic glasses[14] and there is a growing body of work dealing with the production and thermal mobility of H atoms in solid H_2,[20] little has been done to investigate the dynamics of H atoms in rare gas matrices. Since H atoms are the lightest atomic species and thus often exhibit interesting quantum phenomena, this lack of prior work is particularly surprising. We have shown that H atoms are thermally stable in xenon at 10 K for at least a week at mole ratios of approximately 1:10,000.[3] This result was not anticipated in light of prior reports of H atom mobilities in experiments that lead to the production of reactive H atom adducts.[9] The ability to stabilize H atoms and the fact that they can be conveniently produced by photolysis of hydrogen halides[14] motivated a more detailed study of the dynamics of matrix isolated H atoms.

In this work H atoms are produced by photodissociation of HBr in xenon. Both the H atom and the resulting halogen can be probed by laser induced fluorescence from H and halogen rare gas exciplexes. Xenon was chosen as the matrix medium since exciplex emission, originating from a species commonly assigned as Xe_2H, can be induced with conventional laser sources.[21] As indicated above, dissociative relaxation of exciplexes have been shown to result in the formation of translationally excited atoms and thus the possibility of photoinduced mobility and photoinduced reactions resulting from the dissociative relaxation of exciplexes was anticipated. However, another type of photomobilization process is also to be anticipated in this system. The UV photolysis of hydrogen halides has been used to produce translationally excited H atoms in the gas phase.[22] Such a process is also possible in cryogenic rare gas solids, though to our knowledge there have been no prior detailed studies of such processes.

The thermal mobility of H atoms has been studied where these atoms are generated by 193 nm photolysis of HBr. The mobility of these species is shown to be highly temperature dependant and to depend on the morphology of the matrix under study.

C atoms are another potentially important reactive species. We report preliminary work on the generation of C atoms in a low temperature cryogenic environment.

At the beginning of the Contract the PI was involved in completing work from a prior contract on the dynamics of systems in rare gas fluids and the validity of the isolated binary collision model (IBC model) in these systems. This work is reported in reference 4 and will not be discussed in more detail in this report.

EXPERIMENTAL

A detailed description of the experimental procedures can be found in a number of publications.[1-8]

Briefly, the unfocused output of a Questek model 2210 excimer laser was used to irradiate the matrices under study. Unless otherwise stated the laser fluence was 7.1 mJ/cm^2 when

measured in front of the matrix window. This irradiation was at either 193 or 248 nm. 193 nm irradiation of N_2O in the gas phase produces $O(^1D)$ atoms. 193 or 248 nm irradiation of HBr doped matrices resulted in dissociation of HBr and production of H and Br atoms.

Matrices were deposited onto a 2.5 cm diameter, 2 mm thick BaF_2 window attached via an indium gasket to a CTI model 22 refrigerator cold tip. Temperature was controlled using a silicon diode sensor attached to the cold tip and a model 805 temperature controller (Lake Shore Cryotronics). Window temperatures were measured with a second diode mounted directly on the matrix window. The vacuum housing consists of perpendicular sets of windows for laser irradiation and fluorescence detection.

O atom concentrations were monitored by laser induced fluorescence (LIF) around 736 nm, produced upon irradiation of N_2O doped Xe matrices, using a gated optical multichannel analyzer (OMA) (Princeton Instruments model IRY 700) attached to a monospec 27 spectrograph (Jerrel - Ash model 82-499) equipped with a 600 grooves/mm holographic grating. The typical spectrograph slitwidth was approximately 600 μm. A Corning 3-66 filter was placed in front of the slits to reject scattered excimer laser light. The excimer laser and OMA gating electronics were triggered by a Wavetek pulse generator. The trigger delays were adjusted such that the gate on the OMA opened approximately 50 ns before the laser pulse. The gate width (approximately 45 μs) of the OMA was set to be much longer than the fluorescence decay time. The output of the OMA is thus an integration of the fluorescence signal over the entire duration of the fluorescence. LIF signals were corrected for shot to shot variations in the excimer laser output which was monitored with a visible photodiode connected to a LeCroy model 9310 digital oscilloscope. The photodiode monitored the partial reflection of the excimer beam from a CaF_2 window or viewed the light produced by the laser pulse upon striking fluorescent paper mounted directly in front of the photodiode.

Br atoms produced by the 193/248 nm photolysis of HBr were probed using the 308 nm radiation of a XeCl excimer laser at ~ 1.0 mJ/cm^2. The sample was probed subsequent to each photolysis laser pulse and the intensity of Xe_2Br exciplex emission was recorded at 470 $\pm$ 0.5 nm using a 1P28 photomultiplier tube connected to a Stanford Research Systems box car integrator. An IBM compatible personal computer triggered the laser and read the integrated voltage from the box car integrator. The 165 μsec time delay between the photolysis and 308 nm probe pulses was set by a Wavetek pulse generator. This delay which is much larger than the radiative lifetime of Xe_2Br[23] was selected to insure that any Xe_2Br produced by the 193/248 nm photolysis laser pulse was in its ground state before the sample was probed at 308 nm. The intensity of Xe_2Br emission varied linearly with the 308 nm probe laser fluence indicating the formation of Xe_2Br is a result of a single photon process.

H atom concentrations were probed using Xe_2H emission. Xe_2H exciplexes, which absorb in the 6.0-7.0 eV energy region, were excited using the 6.42 eV photons from an ArF excimer laser.[21] Emission at 4.96 eV was detected by a 1P28 phototube connected to a SRS Box Car Integrator or was detected with a Princeton Instruments Gated OMA. The output of either device was fed to an IBM compatible personal computer.

A Mattson Polaris series Fourier transform infrared (FTIR) spectrometer was used to monitor the changes in the infrared absorption spectrum as a result of photolysis. All matrices were deposited at 27 K unless otherwise stated. For experiments conducted at other temperatures, the matrix window was subsequently warmed or cooled to the appropriate temperature. The gas samples used for matrix deposition were premixed in glass bulbs. Xenon (99.995%), obtained

3

from Cryogenic Rare Gas, and N_2O (>99.0%), obtained from Matheson, were used without further purification. NO (99%), obtained from Matheson, was purified by flowing the gas through a column of ascarite which eliminated the NO_2 impurity as judged by FTIR spectroscopy. An NO impurity was eliminated from NO_2 (95.5%), obtained from Aldrich, by distillation. Isotopically labelled $^{15}N^{14}N^{16}O$ (99%) obtained from Cambridge Isotope Laboratories and N_2 (99.998%) obtained from Linde were used without further purification. HBr specified as 99.8% pure was obtained from Matheson and subjected to several freeze pump thaw cycles before use.

RESULTS AND DISCUSSION

O Atoms

Number of 193 nm laser pulses
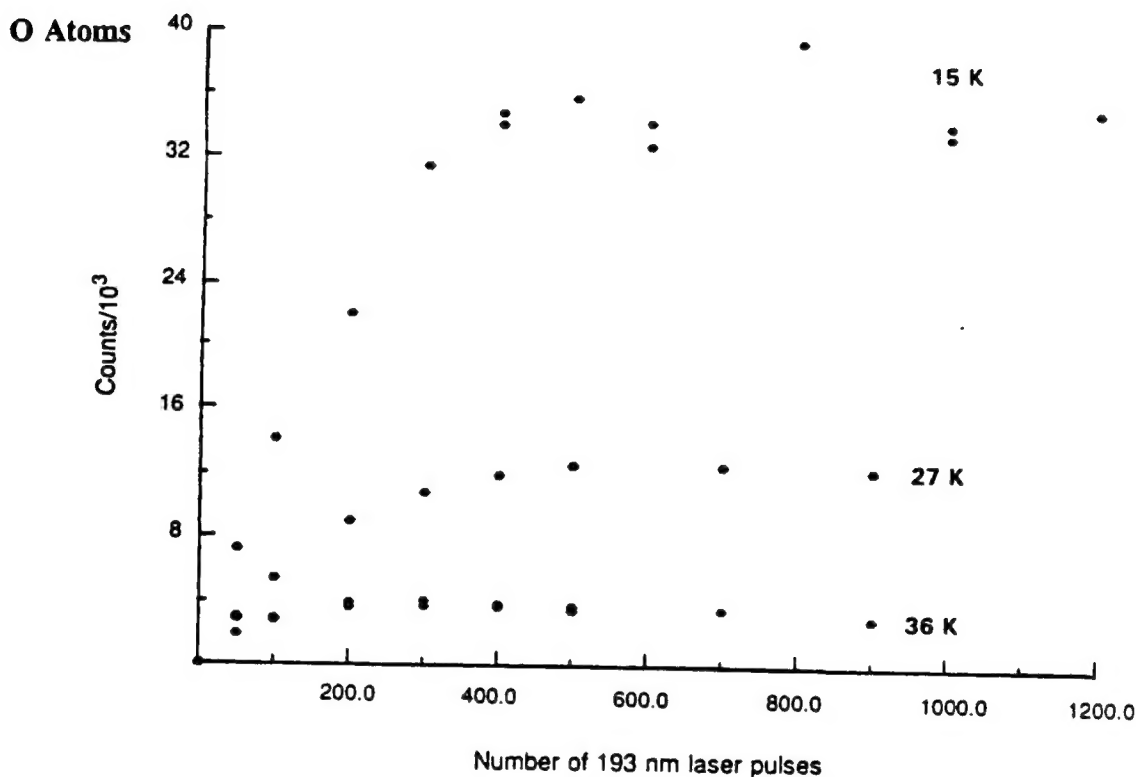
Figure 1

A plot of the O atom photoproduction curve at three temperatures 15, 27 and 36 K

Figure 1 displays typical O atom "photoproduction" curves.[1] These curves are generated by 193 nm photolysis of N_2O doped Xe matrices at various temperatures with the O atom concentration probed by XeO emission. The shape of the curve can be reproduced considering a competition between O atom production

$$N_2O + h\nu_{193} \rightarrow N_2 + O(^1D) \qquad\qquad (\sigma_1\phi_1 I) \qquad\qquad (1)$$
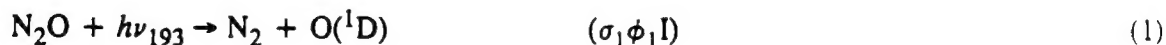
and O atom loss as a result of photoinduced mobility

4

$$O(^1D) + Xe \rightarrow XeO(^1D) \qquad\qquad (k_2) \qquad\qquad (2)$$
$$XeO \rightarrow Xe + O^*(^3P) \qquad\qquad (k_3) \qquad\qquad (3)$$
$$O^* + Xe \rightarrow O + Xe \qquad\qquad (k_4) \qquad\qquad (4)$$
$$Xe + O + h\nu_{193} \rightarrow XeO. \qquad\qquad (\sigma_2 I) \qquad\qquad (5)$$
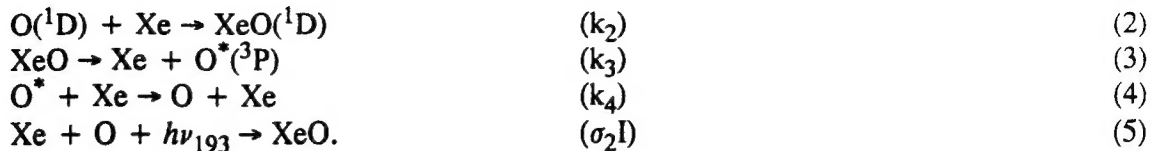
The resulting differential equation for the O atom concentration can be written

$$d[O]/dt = \sigma_1\phi_1 I[N_2O] - 2k\sigma_2 I\Delta t[O]^2 \qquad\qquad (6)$$

or

$$d[O]/dt = \sigma_1\phi_1 I[N_2O]_0 I \exp(-\sigma_1\phi_1 It) - 2k\sigma_2 I\Delta t[O]^2. \qquad\qquad (7)$$

An analytical solution exists for this differential equation and has the form

$$[O] = [N_2O_2]_0\sqrt{\tau/k'} \left\{ \frac{iJ_1[2i\sqrt{(k'\tau)}]] - \beta'H_1^{(1)}[2i\sqrt{(k'\tau)}]}{J_0[2i\sqrt{(k'\tau)}] + \beta'H_1^{(1)}[2i\sqrt{(k'\tau)}]} \right\} \qquad\qquad (8)$$

Although an analytical solution exists, it was more convenient to fit the experimental data to asymptotic forms of the solution or to numerically integrate the above equations. From the prior equations and mass balance one obtains

$$d[O]/dt = \sigma_1\phi_1 I[N_2O]_0 - \sigma_1\phi_1 I[O] - (\sigma_1\phi_1 I/2)[O_2] - 2k\sigma_2 I\Delta t[O]^2 \qquad\qquad (9)$$

In the early time limit the O_2 term will not be significant and this equation reduces to

$$d[O]/dt = \sigma_1\phi_1 I[N_2O]_0 - \sigma_1\phi_1 I[O] - 2k\sigma_2 I\Delta t[O]^2 \qquad\qquad (10)$$

The analytical solution for this differential equation is of the form

$$[O] = \beta \tanh(\gamma + t/\tau) - \varepsilon \qquad\qquad (11)$$

The data can be well fit with this form of the solution. Alternatively, as shown in Figure 2, a Runge-Kutta method can be used to numerically integrate the relevant differential equations. The fit in Figure 2 was generated for $\phi_1\sigma_1 = 6.0 \times 10^{-20}$ cm^2 and $k\sigma_2 = 1.1 \times 10^{-29}$ cm^{5}s^{-1}.

The cross-section for photodissociation of N_2O in Xe was found to be 6.4×10^{-20} cm^2 at 27 K, comparable to the gas phase value of 1.1×10^{-19} cm^2 [14] suggesting an inefficient cage effect. This cross-section decreases approximately 10% for every 10 K increase in temperature.

As shown in Figure 3 the 214-293 nm ultraviolet absorption spectrum of the XeO complex reveals a single peak centered at 249 nm with no apparent vibrational structure. The absorption cross-section at 249 nm was determined to be 1.9×10^{-16} cm^2.
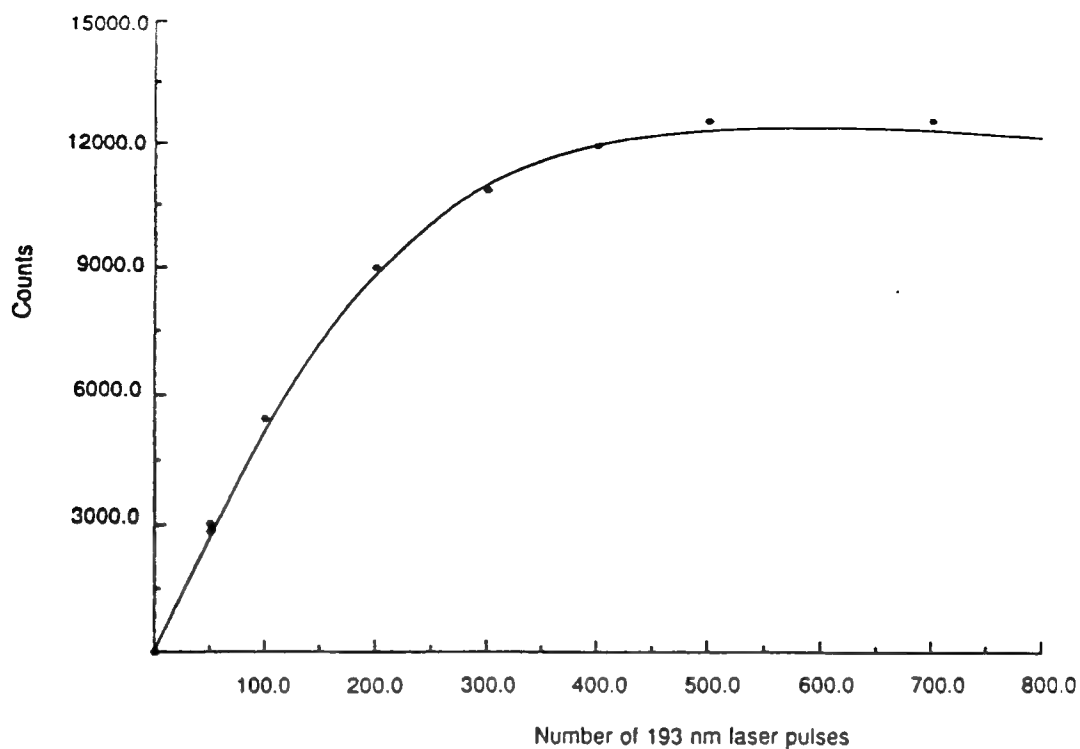
Figure 2

The experimental O atom production curve at 27 K for a 1:794 N_2O doped Xe matrix obtained by monitoring 736 nm XeO emission vs the number of 193 nm laser pulses with the line generated by numerical integration of equation 7.
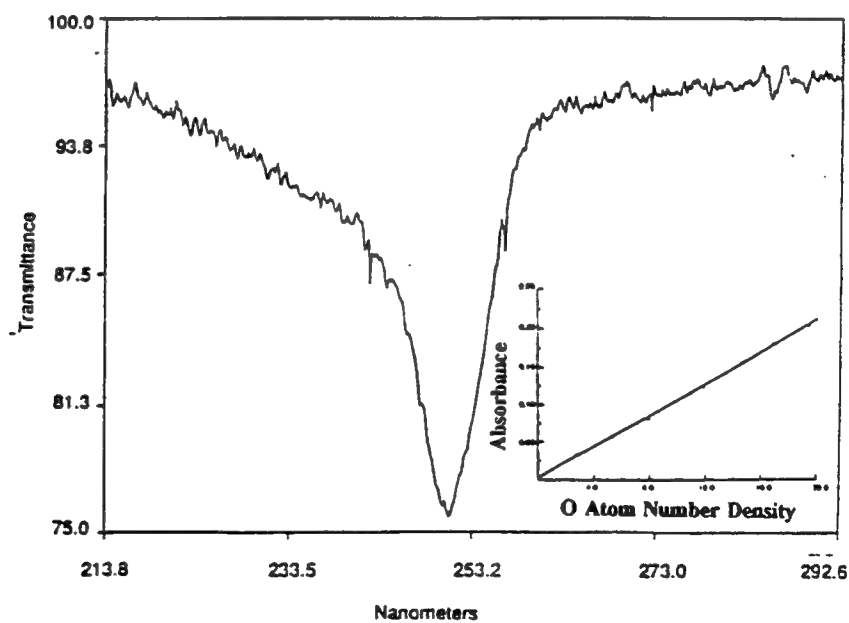
Figure 3

The UV spectrum of XeO from 214-293 nm in a 1:794 N_2O:Xe matrix at 15 K obtained after 450 193 nm laser pulses. The inset is a Beer's law plot of the 249 nm absorbance vs O atom number density in units of 10^{17} atoms/cm^3 calculated as discussed in the text.

6

The temperature dependance of the data in Figure 1 demonstrates that the rate of O atom production and the shape of the O atom production curves are a result of a competition between O atom photolytic production and O atom loss as a result of photomobilization leading to O + O recombination. The data implies that even though there is a modest increase in the photodissociation cross-section, the steady state level for O atoms increases at lower temperatures primarily due to a strong temperature dependance of the loss process: becoming much less efficient at lower temperatures.

O atom photodepletion can be studied independent of the photoproduction process. This has been accomplished by production of O atoms using 193 nm photolysis and photomobilization at 248 nm.[2] At this latter wavelength N_2O is not significantly dissociated. As shown in Figure 4, the steady state populations produced by 193 nm irradiation can be depleted by 248 nm irradiation.

Number of 248nm Laser Pulses
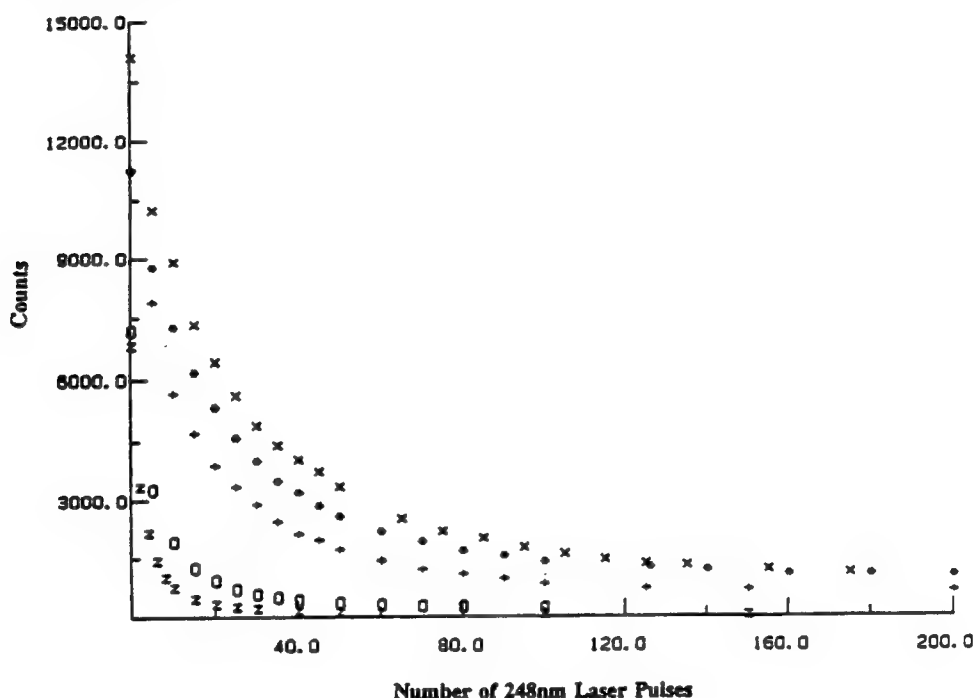
Figure 4

The O atom photodepletion curve at five temperatures: 15K(x), 20K(∗), 27K(+), 36K(o), 42K(z).

The relevant kinetics for the process are as follows. Equation (12) describes the absorption of light by O/Xe pairs which results in the creation of an XeO complex which ultimately dissociates producing mobile O atoms designated as O^*:

$$O/Xe + h\upsilon \rightarrow XeO \rightarrow O^* + Xe \qquad \sigma n \qquad (12)$$

If a small fraction of the initial ensemble of O atoms are excited then the number density of mobile O atoms created within the laser pulse can be approximated by the relation

7

$$[O^*] = n\sigma[O] \tag{13}$$

where n is the laser intensity in units of photons cm^{-2} $pulse^{-1}$ and σ is the XeO charge transfer absorption cross-section. Given that $[O^*] << [O]$, recombination can be assumed to occur at stationary sites:

$$O^* + O \rightarrow O_2 \qquad\qquad k_e \tag{14}$$

with an effective rate constant (k_e) (most generally this will be a rate coefficient). The phenomenological rate equation for this process can then be written in terms of the number of laser pulses N, as:

$$\frac{d[O]}{dN} = -2\sigma n k_e[O]^2 \tag{15}$$

where k_e has the units of cm^3. To gain further insight into the kinetic process and the microscopic meaning of k_e, equation 15 can be derived in a different way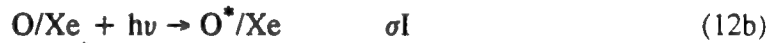 using only equations 12 and 14, rewritten assuming a steady state concentration of O^*, all travelling with the same velocity (v):

$$O/Xe + h\upsilon \rightarrow O^*/Xe \qquad\qquad \sigma I \tag{12b}$$
$$O^* + O \rightarrow O_2 \qquad\qquad k \tag{14b}$$

where the bimolecular rate constant k can now be written as $k = v\sigma_r$ and $\sigma_r = \pi r^2$ (2r is defined as the distance between adjacent substitutional sites) and the laser fluence I is in units of photons cm^{-2} s^{-1}. The rate equation for production of O atoms is then

$$\frac{d[O^*]}{dt} = \sigma I[O] \tag{16}$$

and the rate equation for loss of O atoms is

$$\frac{d[O^*]}{dt} = -v\sigma_r[O^*][O] \tag{17}$$

If the laser pulse is treated as a delta function, $I(t) = n\delta(t)$, where n is $photons/cm^2$ and $[O^*] << [O]$, then equation 16 can be integrated to yield

$$[O^*]_o = n\sigma[O] \tag{18}$$

which is the number of O^* created per pulse. Therefore, the number of O atoms lost per pulse is $2n\sigma[O]$ and

$$\frac{d[O]}{dN} = -2n\sigma[O] \tag{19}$$

which represents a *first order* kinetic process. In this picture all O^* that are created react and since the creation of O^* is first order with respect to the N_2O concentration, a first order loss process

8

is expected. This result is similar to that developed in a previous study of the kinetics of exciton transport.[24] Second order kinetics results when O^* quenching processes are important in addition to reactive loss. The inclusion of quenching processes can conveniently be accomplished by introducing a velocity decay term representing a first order quenching process:

$$v = v_o e^{-\gamma t} \tag{20}$$

where $\gamma = 1/\tau$ and τ represents the lifetime of O^* atoms which are quenched. Velocity relaxation will result from the loss of kinetic energy of the O^* to the phonon bath of the matrix as the O atom travels through the matrix and interacts with Xe atoms. Introducing equation 20 into equation 17 and integrating between the limits of 0 and ∞, where ∞ is defined as less than the time between pulses, yields:

$$[O^*]_\infty = [O^*]_o e^{\frac{-v_o \sigma_r [O]}{\gamma}} \tag{21}$$

where $[O^*]_\infty$ is the number of O^* that react after a given laser pulse. The efficiency of reaction per pulse, f, is therefore

$$f = \frac{[O^*]_o - [O^*]_\infty}{[O^*]_o} = 1 - e^{\frac{-v_o \sigma_r [O]}{\gamma}} \tag{22}$$

and the number of O atoms lost per pulse is then

$$2[O^*]_o f = 2n\sigma[O]f \tag{23}$$

Retaining the first term in the expansion of the exponential in equation 22, the O atom loss rate equation can be written as

$$\frac{d[O]}{dN} = -2n\sigma\left(\frac{v_o \sigma_r}{\gamma}\right)[O]^2 \tag{24}$$

By comparing equation 24 to equation 15, it follows that:

$$k_e = \left(\frac{v_o \sigma_r}{\gamma}\right) \tag{25}$$

Thus k_e represents the reactive volume swept out by the mobile atom subsequent to its creation and prior to reaction. As derived in reference 25, k_e can also be set equal to $\ell\sigma_r$. The length ℓ is the total distance travelled by the mobile atom and represents an upper limit to the displacement of the atom from its point of origin. The relationship between ℓ and the actual displacement from the point of origin depends upon the microscopic environment in which the atom moves (*i.e.* site hopping versus channeled movement versus long range defects, etc.). The physical meaning of ℓ is therefore dependent on the microscopic morphology of the host material. Since k_e represents the occluded volume of the matrix swept out by the mobile atom, it can be related to a reaction probability and directly compared to experimental results.

The above kinetic model, while illustrative of how the effective rate constant relates to distance travelled by the mobile atom, includes several simplifying assumptions such as the instantaneous production of mobile atoms, and the assumption that $[O^*] << [O]$. In the present work these assumptions are not always valid. Thus to adequately describe the experimental results, a more general treatment is required.

The following minimal set of equations is necessary to more accurately describe the O atom loss mechanism:

$$Xe + O + h\upsilon \rightarrow XeO \qquad\qquad \sigma I \qquad\qquad (26)$$
$$XeO \rightarrow Xe + O^* + h\upsilon \qquad\qquad k_{27} \qquad\qquad (27)$$
$$O^* + Xe \rightarrow O + Xe \qquad\qquad k_{28} \qquad\qquad (28)$$
$$O^* + O \rightarrow O_2 \qquad\qquad k \qquad\qquad (29)$$
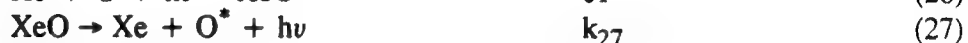
An estimation of the reaction probability from the data in Figure 4 coupled with a calculation of the concentration of excited O^* based on the known absorption cross-section for XeO[1] indicates that, at least at low temperature (where only a few percent of the O^* react/pulse), the majority of O^* created are relaxed prior to reaction. Therefore $O^* + O^*$ recombination is not expected to be significant. The addition of this process to the kinetic scheme significantly complicates the kinetic description of the system. Since we have justified neglecting this process at lower temperatures and the kinetic description we develop appears to describe the observed kinetics for all temperatures, we feel justified in excluding this process at all temperatures. The loss of O atoms is then related to the rate of formation of O_2 by:

$$\frac{d[O_2]}{dt} = -\frac{1}{2}\frac{d[O]}{dt} = k[O][O^*] \qquad\qquad (30)$$

The processes in equations 28 and 29 are expected to be much faster than the process in equation 27 resulting in a steady-state $[O^*]$ concentration.[26] With this assumption, the steady-state solution for $[O^*]$ is:

$$[O^*] = \left(\frac{k_{27}}{k_{28} + k[O]}\right)[XeO]_0 e^{-k_{27}t} \qquad\qquad (31)$$

where $[O^*]$ has been related to the initial exciplex concentration, $[XeO]$. Substituting equation 31 into equation 30 yields a general rate equation for the system:

$$\frac{d[O]}{dt} = -2\left(\frac{kk_{27}}{k_{28} + k[O]}\right)[XeO]_0[O]e^{-k_{27}t} \qquad\qquad (32)$$

In the limit where $k[O] >> k_{28}$ (i.e., quenching is insignificant so every O^* reacts) equation 32 becomes

$$\frac{d[O]}{dt} = -2k_{27}[XeO]_0 e^{-k_{27}t} \qquad\qquad (33)$$

10

Integrating this expression between the limits of 0 and ∞, where ∞ is less than the time between laser pulses, and substituting $[XeO]_0 = \sigma n[O]_0$ yields

$$[O]_0 - [O]_\infty = 2\sigma n[O]_0$$

The efficiency of reaction, f, can be written as:

$$f = \frac{[O]_0 - [O]_\infty}{[O]_0} = 2\sigma n \tag{34}$$

The loss rate of O atoms per laser pulse is first order and given by

$$\frac{d[O]}{dN} = -[O]f = -2\sigma n[O] , \tag{35}$$

the same result as derived in equation 19.

Alternatively, in the limit of $k_{28} >> k[O]$ (*i.e.*, O atom quenching dominates reaction) equation 31 becomes:

$$\frac{d[O]}{dt} = -2\left(\frac{kk_{27}}{k_{28}}\right)[XeO]_0[O]e^{-k_{27}t} \tag{36}$$

Integrating between the limits of o and ∞ again, yields

$$\ell n\left(\frac{[O]_\infty}{[O]_o}\right) = \frac{-2kk_{27}[XeO]_0}{k_{28}}\int_o^\infty e^{-k_{27}t}\,dt \tag{37}$$

therefore

$$[O]_\infty = [O]_o\, e^{-2\frac{k}{k_{28}}[XeO]_o} \tag{38}$$

The efficiency of reaction, f, is then

$$f = 1 - e^{-2\frac{k}{k_{28}}[XeO]_o} \tag{39}$$

Retaining the first term in the expansion of the exponential in equation 39, the following equation for O atom loss per pulse is obtained:

$$\frac{d[O]}{dN} = -2\left(\frac{k}{k_{28}}\right)[XeO]_o[O] \tag{40}$$

The initial XeO concentration, $[XeO]_o$, produced by a laser pulse of pulsewidth Δt, can be determined from equation 25 using Beers's law and neglecting XeO loss during the laser pulse as:

$$[XeO]_o = [O](1 - e^{-\sigma n}) \tag{41}$$

Substituting equation 36 into equation 35 yields:

11

$$\frac{d[O]}{dN} = -2\left(\frac{k}{k_{28}}\right)(1 - e^{-\sigma \eta})[O]^2 \tag{42}$$

Assuming the expansion of the exponential in equation 37 can be adequately represented by the first term, the following O atom loss equation is obtained:

$$\frac{d[O]}{dN} = -2\left(\frac{k}{k_{28}}\right)\sigma \eta [O]^2 \tag{43}$$

Comparing this equation to equations 24 and 25 the relationship between the effective experimental rate constant and the volume swept out by the O atom is again apparent:

$$k_e = \frac{k}{k_{28}} = \frac{v_o \sigma_r}{\gamma} \tag{44}$$

where $k = v_o \sigma_r$ as defined earlier and γ is equivalent to the quenching rate constant k_{28}.

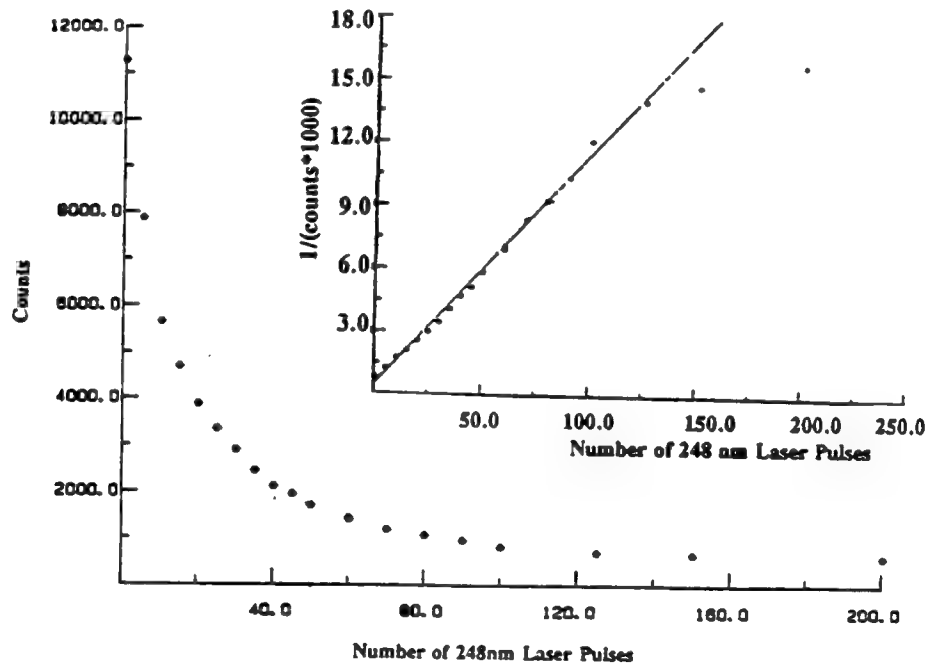Figure 5

The experimental O atom photodepletion curve (*) at 27 K (1:794 N_2O doped Xe matrix) obtained by monitoring the 736 nm XeO emission verses number of 248 nm laser pulses. The inset contains the data plotted as the inverse of the OMA counts verses the number of 248 nm laser pulses. The line is a least squares fit to the first 17 data points which correspond to the first 122 laser pulses.

Thus the kinetic expressions derived above predict that O atom loss will be first order when $k[O] >> k_{28}$ and second order in $[O]$ when $k_{28} >> k[O]$. In between these limits there will be a transition regime where the O atom concentration will initially decay with first order kinetics and evolve into a second order decay as the $[O]$ decreases and thus k_{28} becomes $>> k[O]$. As shown in Figure 5 the data obtained for O atom loss at 27 K yields a linear plot of $1/[O]$ versus laser pulses (what is actually plotted is 1/counts, where counts are proportional to O atom concentration) indicative of second order kinetics. Deviations from linearity are observed after depletion of $>90\%$ of the initial O atom population. We believe these deviations result from a distinct population of O atoms which are less mobile and thus display different kinetics for reactive loss. Data for loss of O atoms between 15 and 42 K all exhibit similar behavior indicative of second order loss of O atoms. Data at 42 K produces a somewhat poorer fit to a second order plot. To determine if this poorer fit was due to the onset of first order kinetics, we numerically integrated equation 32, the general rate equation for O atom reactive loss. Since the $[O]$ is known, the values for k_e are tabulated in Table 1, the ratio between k and k_{28} can be determined (see equation (34)). Once the results of numerical integration of equation 32 are fit to data at one temperature, signals can be generated at other temperatures based purely on changes in the magnitude of $k[O]$ versus k_{28} where the relative magnitude of these two terms as a function of temperature is determined by the experimental measurement of k_e. A comparison between the experimental data and the results of numerical integration of equation 32 at 35 and 42 K indicates that there is some evidence of an initial first order loss process in the 42 K data. However, even at 42 K the loss process rapidly

Table 1. **Effective Rate Constants for Photoinduced Loss at the Temperatures and Fluences Studied**

Temperature in (K)	k_e (cm^3) ($\times 10^{20}$)[a]	Fluence in (mJ/cm^2)
15	13	7.1
20	17	7.1
27	28	7.1
36	142	7.1
42	323	7.1
27	12	3.6
27	27	7.8
27	24	13.9

a. Error limits on k_e are typically $\pm 15\%$ or less.

13

becomes second order and only the initial few points in the experimental signal may be perturbed by the first order loss process. This behavior is indicative of the beginning of a transition to first order kinetics. As expected, as the [O] atom concentration is depleted, the loss process reverts to second order behavior. For all lower temperatures the simulations indicate that the data can be treated as strictly a second order decay of O atoms.

We now consider the application of the derivation of the kinetics for O atom loss to 248 nm irradiation experiments. The derivation of equation 43 is valid for 193 nm laser irradiation. That is, the argument of the exponential is small enough that it is sufficient to retain only the first term in the Taylor series expansion. This conclusion is based on the results of our previous study of N_2O doped Xe matrices, which determined k_e and σ at 27 K to be 6.9×10^{-21} cm^3 and 2.4×10^{-17} cm^2 respectively.[1] Analogous to the treatment used by Apkarian, if k_e is expressed as $\ell\sigma_r$ and $\sigma_r = 1.5 \times 10^{-15}$ cm^2, a value of ℓ of 460 Å is calculated at 27 K.[25] This represents an upper limit to the displacement of the mobile atom.

The assumption used in the derivation of equation 43 is not valid for 248 nm laser irradiation since the argument of the exponential in equation 42 is no longer small enough to retain only the first term in the Taylor series expansion at the fluences used in this study. Equation 43 indicates that the slope of the bimolecular curves should be linear in laser fluence. The laser fluence dependance of the O atom loss curves shown in Table 1 indicates the excitation step shown in equation 26 is nearly saturated at the 248 nm photolysis fluences used in this study. This result is expected based on the measured absorption coefficient for the formation of XeO exciplexes and the laser fluence employed in these experiments.[1] In this limit, the initial Xe^+O^- concentration can be approximated as

$$[XeO]_o \approx \frac{[O]}{2} \tag{45}$$

Substituting into equation 40, a rate equation is obtained which describes the O atom loss data:

$$\frac{d[O]}{dN} = -\left(\frac{k}{k_{28}}\right)[O]^2 = -k_e[O]^2 \tag{46}$$

where k_e equals the slope of the bimolecular plots of the data in Figure 3. The values of k_e for the data in Figure 3 are tabulated in Table 1. The value of k_e at 42 K is taken from the second order portion of the decay curve. As previously indicated, numerical integration of equation 32 using these k_e's produces curves that fit the data.

O Atom Reactions

Since the reaction of $O(^1D)$ with N_2 to form N_2O is spin allowed, a nitrogen matrix provides a medium in which reactions of photogenerated $O(^1D)$ can potentially occur. That the reaction does occur is demonstrated by the results displayed in Figure 6. Upon 193 nm photolysis of an N_2O (546)/N_2 matrix, the peak at 2235 cm^{-1}, corresponding to the ν_3 mode of $N_2O(446)$, grows in. A small peak at this wavelength in the spectrum of the unphotolyzed matrix is due to an $N_2O(446)$ impurity in the sample. Based on the rate of loss of $N_2O(546)$ and the rate of formation of $N_2O(446)$ the quantum yield for reaction of O atoms with N_2 was determined to be

14

~0.06. Though this reaction is known in the gas phase it is normally dominated by efficient quenching of $O(^1D)$ to $O(^3P)$. Previously the highest yields for this reaction were in condensed phase with a reported quantum yield in liquid N_2 of 0.014.[27] These results imply that the N_2 matrix environment is more efficient at stabilizing internally excited N_2O^* formed by reaction or less efficient at deactivating $O(^1D)$ or both.
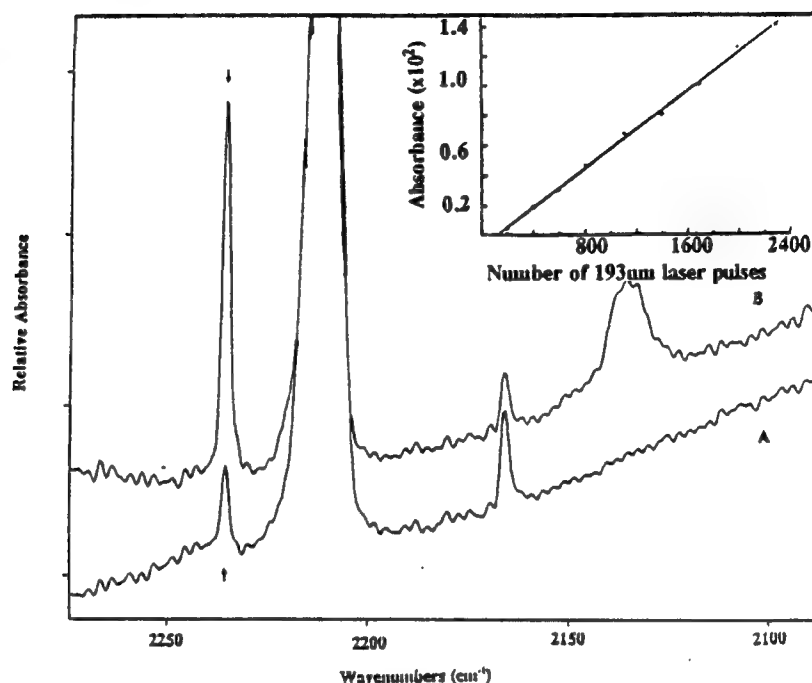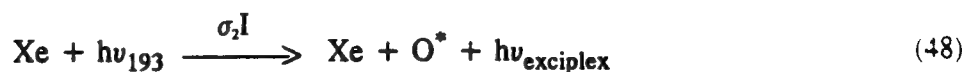

Figure 6

A displays an infrared spectrum of an unphotolyzed $N_2O(546)/N_2$ (1:354) matrix deposited at 15 K. The (546), ν_3, monomer absorption is at 2213 cm^{-1}. The absorptions at 2166 and 2235 cm^{-1} are due to (556) and (446) impurities respectively. 6B displays the same matrix after irradiation with 1800 193 nm laser pulses. The (546) and (556) absorptions decrease upon photolysis while the (446) absorption (marked by the arrows) grows. An ozone absorption $(2\nu_1)$ also grows in at 2135 cm^{-1}. The inset displays a plot of ozone absorption intensity versus the number of 193 nm laser pulses.

As shown in Figure 7, the photoproduction curves for doping ratios of (1:100) and (1:26) have faster rises and higher plateau levels than the (1:794) doped matrices. The solid lines in this figure were generated using the kinetic model developed in reference 1. Briefly, that model includes three essential equations
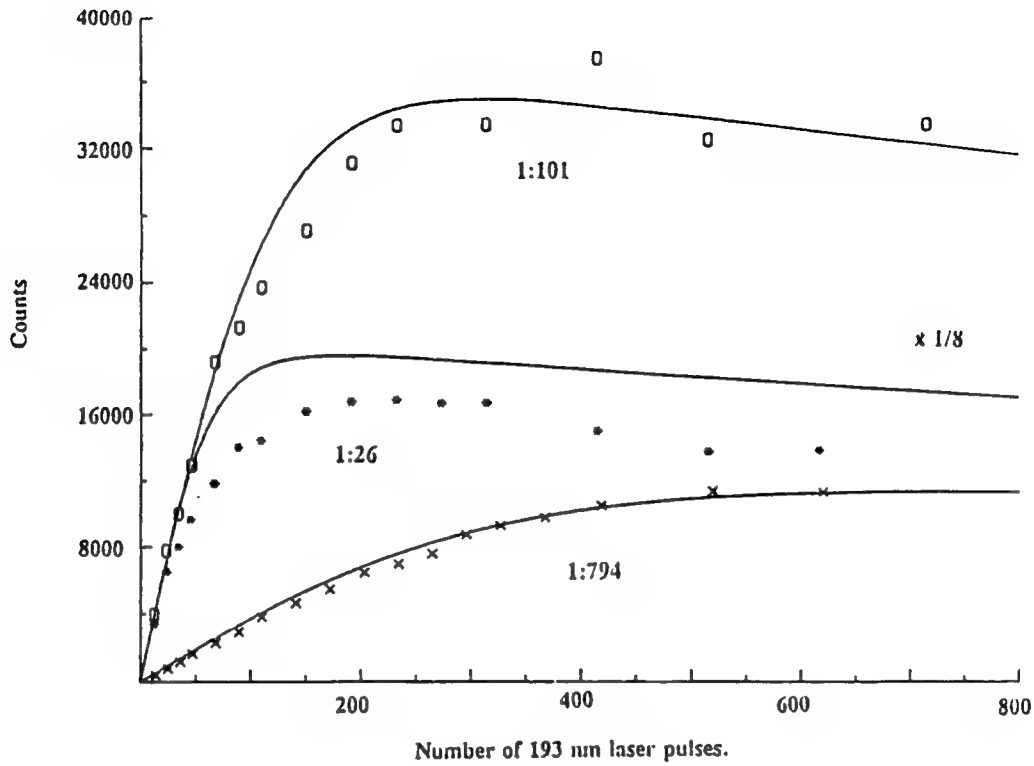
$$N_2O + h\nu_{193} \xrightarrow{\phi,I} N_2 + O \tag{47}$$

$$Xe + h\nu_{193} \xrightarrow{\sigma,I} Xe + O^* + h\nu_{exciplex} \tag{48}$$

$$O^* + O \xrightarrow{k} O_2 \tag{49}$$

15

Figure 7

O atom photoproduction curves obtained at 10 K by 193 nm photolysis of N_2O/Xe matrices with doping ratios: (1:794) (*), (1:101) (x) and (1:26) (o). The solid lines were generated by numerically integrating equation 4 varying only the initial N_2O concentration to match the experimental doping ratios. The predicted fit to the (1:26) data was scaled by a factor of 8 so it would not be off the scale of the plot.

from which the following rate expression for the time evolution of the O atom concentration can be derived:

$$d[O]/dt = \sigma_1\phi_1 I[N_2O]_o \exp(-\sigma_1\phi_1 It) - 2k\sigma_2 I\Delta t[O]^2 \qquad (50)$$

where σ_1 is the 193 nm N_2O absorption cross-section, ϕ_1 is the O atom cage exit quantum yield, σ_2 is the 193 nm XeO absorption cross-section, k is the rate constant for bimolecular recombination of O atoms in units of cm^3/s, the product $\sigma_1\phi_1$ is the cross-section for photoproduction of O atoms from N_2O photolysis, I is the fluence/pulse in units of photons/cm^2 s and Δt is the laser pulsewidth. The solid lines through the data in Figure 7 were generated by numerically integrating equation (50) using the Runge-Kutta method. The parameters used to generate the curve through the (1:794) data were $\sigma_1\phi_1 = 7.6 \times 10^{-20}$ cm^2, $k\sigma_2 = 4.5 \times 10^{-30}$ cm^5/s and $[N_2O]_o = 2.19 \times 10^{19}$ molecules/cm^3. These parameters are in excellent agreement with those used in reference 1 and reproduce the (1:794) data shown in Figure 6. The solid line through the (1:101) data was generated using the same parameters changing only the value of

16

$[N_2O]_o$ to 1.72×10^{20} molecules/cm^3 to match the experimental conditions. This curve closely tracks the (1:101) data missing only slightly in the 100 - 200 pulse region. The fit to the 1:101 and to data generated in prior work on 1:397 matrices[1] matches the shape of the O atom production curve and accurately reproduces the absolute magnitude of the exciplex emission once the proportionality factor between emission and O atom concentration is established based on data from the 1:794 matrix. Interestingly, the predicted curve for the (1:26) data, obtained by using an $[N_2O]_o$ of 6.68×10^{20} molecules/cc, predicts a much higher O atom concentration than observed: so much so that it would be off the figure. The O atom concentration generated in the N_2O:Xe (1:794) matrix is ~ 8 mmolar and is ~ 32 mmolar in the N_2O:Xe (1:101) matrix.
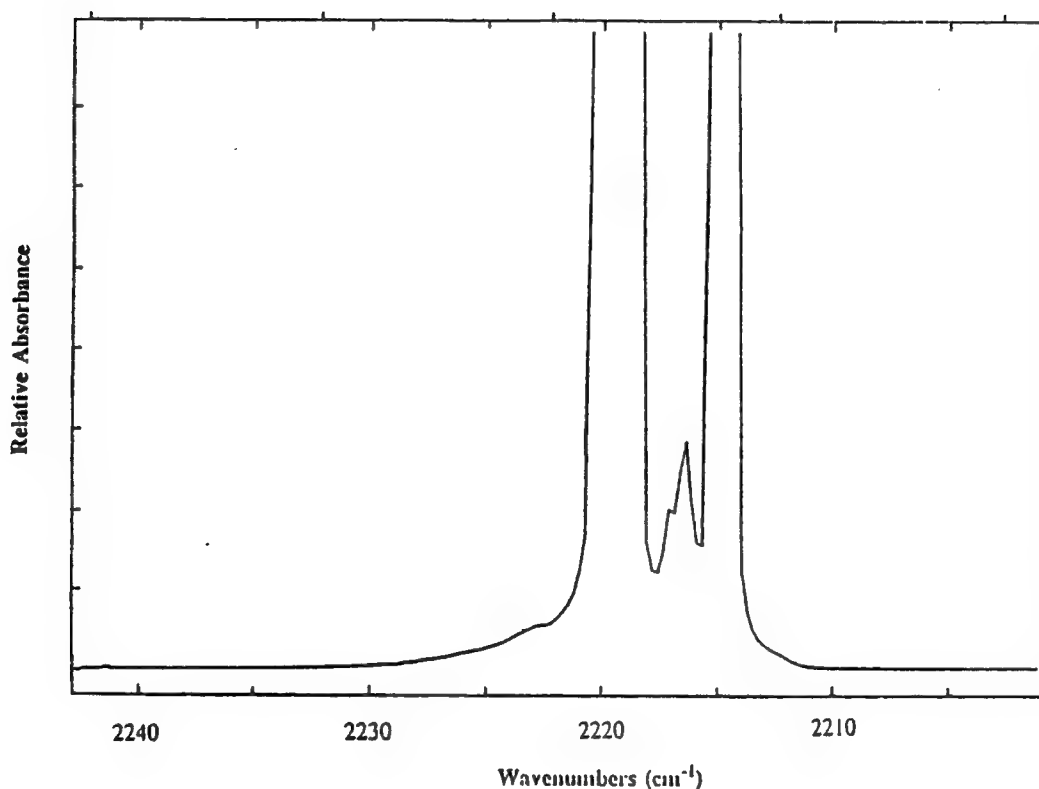

Figure 8

An infrared spectrum of an N_2O:Xe (1:101) matrix at 10 K; deposited at 27 K. The spectrum displays the N_2O, ν_3, monomer band at 2214 cm^{-1} and multimer absorptions.

17

Changes in the infrared spectrum of the 1:26 matrix provides clues to the cause of the deviation from predictions of the model based on equations 47-49. FTIR spectra indicate that multimer formation is negligible at a 1:794 (see references 1 and 15) doping ratio but starts to become significant at higher doping ratios. Figure 8 shows a very strong, ν_3, monomer absorption at ~2214 cm^{-1}, which has been truncated, and a very strong multimer absorption at ~2200 cm^{-1}. A weaker multimer absorption is seen at ~2216 cm^{-1}.

Evidence in the literature points to efficient quenching of O (^{1}D) atoms before they can move significant distances in a Xe matrix.[1,28] Thus it is not surprising that O atom chemistry was not observed in a 1:794 N$_2$O:Xe matrix since the O atom is expected to be deactivated before it can reach a site of another N$_2$O molecule.

However, in matrices doped with large amounts of N$_2$O, multimer formation occurs and the situation regarding O atom chemistry is potentially quite different. In this case, O(^{1}D) atoms may be produced adjacent to other N$_2$O molecules and may react before being quenched by xenon. O atom reactions with N$_2$O within multimers would lead to a reduction in the yield of kinetically and thermally stable O atoms and a deviation from the predictions of equation 50 which does not include these reactive channels. A neat N$_2$O matrix was used as a limiting case of a highly doped system and demonstrated the production of new peaks in the IR spectrum on an irradiated matrix that were compatible with O (^{1}D) chemistry. In particular there was evidence for formation of NO, NO$_2$ and the trans isomer of (NO)$_2$.[29]
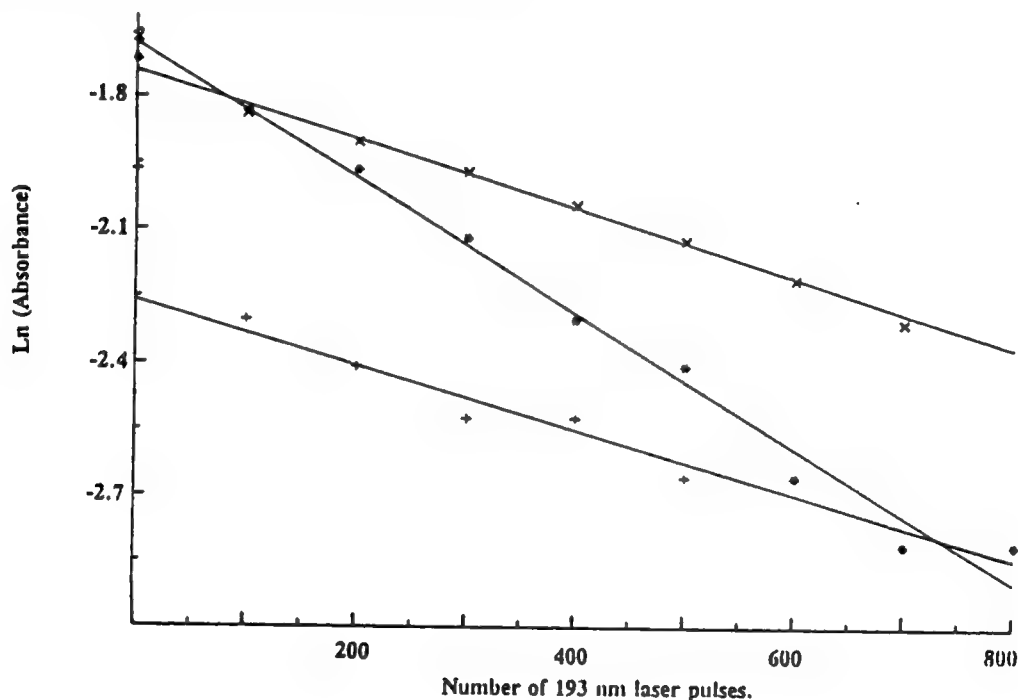

Figure 9

Plots of the natural log of the N$_2$O(446) ν_3 mode absorbance (2214 cm^{-1} in a xenon matrix) versus number of 193 nm laser pulses for N$_2$O(446)/Xe (1:794) matrices deposited at 15 K (*), 27 K (x) and 36 K (+). After deposition, the matrix temperature was adjusted to the experimental temperature of 27 K.

18

A number of studies have shown that photodissociation efficiency is influenced by matrix morphology.[30,31] Figure 9 displays the N_2O loss rate monitored at 27 K, for matrices deposited at 15 K, 27 K, and 36 K. Consistent with what was observed for the HBr/Xe system,[6] N_2O photodissociation has a larger cross-section in the matrix deposited at 15 K than in the matrix deposited at 36 K. While the 36 K deposition data appears to have a slightly smaller cross-section for N_2O loss than the 27 K deposition data, there is no significant difference within the error limits of the experiment. Higher deposition temperatures have been associated with more crystalline matrices.[32] Less efficient dissociation in a more crystalline matrix suggests a greater degree of "in-cage" recombination may be occurring. Evidence of this is seen in Figure 10 which displays the infrared spectrum of an $N_2O(546)/Xe$ (1:350) matrix, deposited at 36 K, before and after photolysis. The small absorption peak at 2169 cm^{-1} which grows in upon photolysis is where the $N_2O(456)$, ν_3, absorption is expected. The 2169 cm^{-1} peak was not observed to grow in on photolysis for matrices deposited at 27 K. Since the observed $N_2O(456)$, ν_3, peak in Figure 10 is just above the signal to noise of the FTIR, its absence in the 27 K deposition data cannot be used to totally rule out "in-cage" recombination. However, since the photodissociation cross-sections for 27 K deposition are close to those for gas phase N_2O at 193 nm, significant in-cage recombination is unlikely.
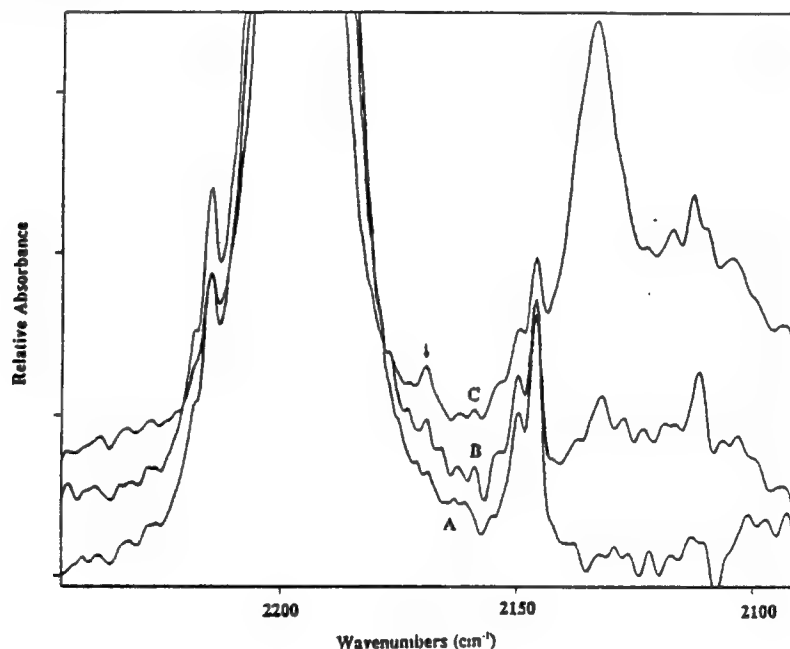
Figure 10

10A displays an infrared spectrum of an unphotolyzed N_2O (546)/Xe (1:350) matrix deposited at 36 K. The (546), ν_3, monomer absorption is at 2192 cm^{-1} while the absorptions at 2147 and 2223 cm^{-1} are due to (556) and (446) impurities respectively. 10B and 10C display spectra of the same matrix after 193 nm photolysis (1.2 mJ/cm^2) for 2186 and 7740 laser pulses respectively. The absorption at 2169 cm^{-1} (marked by the arrow) is due to (456) and grows in upon photolysis. An ozone absorption ($2\nu_1$) at 2133 cm^{-1} also grows in.

19

H Atoms

HBr. Figures 11-14 indicate that, for the matrices under study, the photolytic loss of HBr and the photolytic production of Br atoms at 193 nm are second order in the HBr concentration even though HBr dissociation is initiated by a single photon process.[6] This second order behavior suggests that two HBr molecules are lost and two Br atoms are produced for each photon absorbed by an HBr molecule. This further implies that the loss of the second HBr molecule must be the result of a reaction. Since our results demonstrate the lack of thermal mobility of HBr and thermal and photoinduced mobility of Br atoms under experimental conditions, the only species that remains which is potentially mobile and thus can undergo reactions with HBr molecules is H atoms. The reaction

$$H + HBr \rightarrow H_2 + Br \tag{51}$$
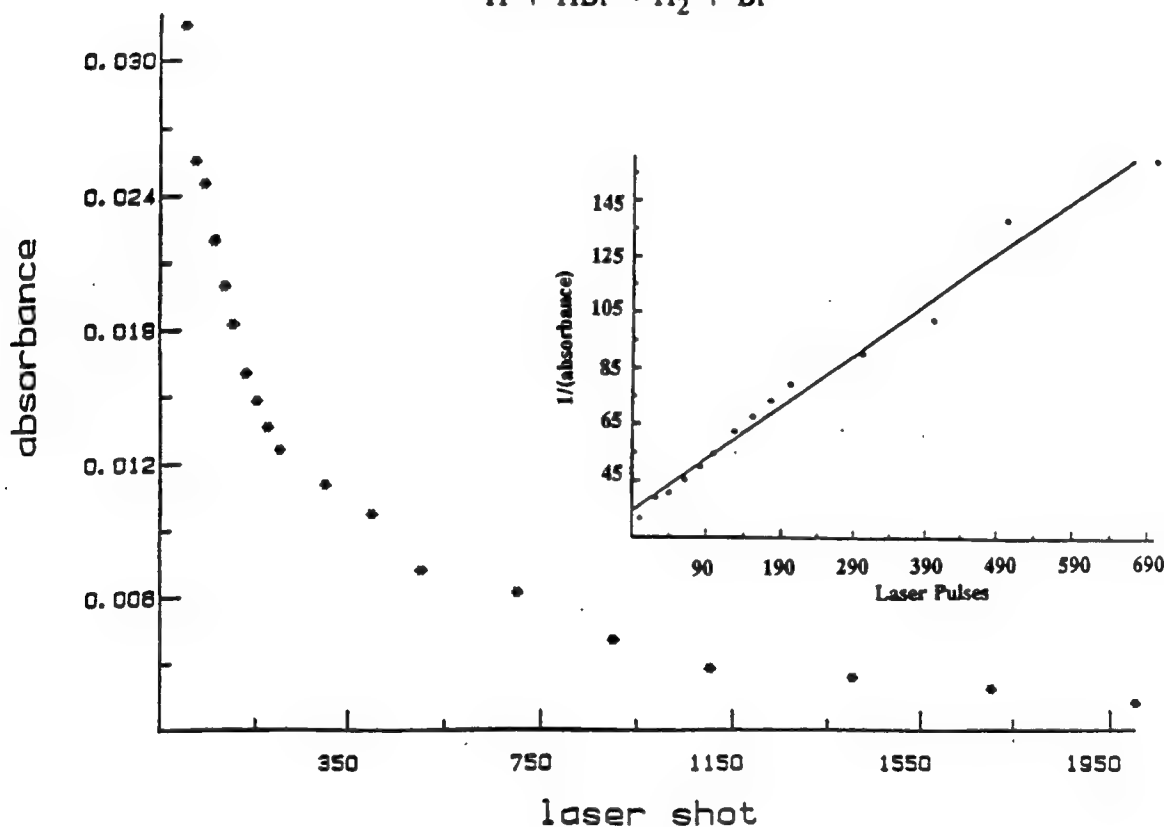

Figure 11

The peak absorbance of the R branch of the HBr monomer at 2508.4 cm^{-1} in a 1:800 HBr:Xe matrix plotted versus the number of 193 nm laser pulses. A complete spectrum was recorded for each data point. The sample was photolyzed at 10 K using a laser fluence of 7.0 mJ/cm^2. $1/(I_{max}-I)$ versus the number of 193 nm laser pulses is shown as an insert.

20

has been studied in the gas phase and is reported to have an activation energy that ranges from slightly negative to -2.5 kcal/mole.[33] The net effect of a reaction mechanism involving photodissociation of one HBr molecule and reactive loss of another would be:

$$2HBr + h\nu_{193} \xrightarrow{k_1} H_2 + 2Br \qquad (52)$$
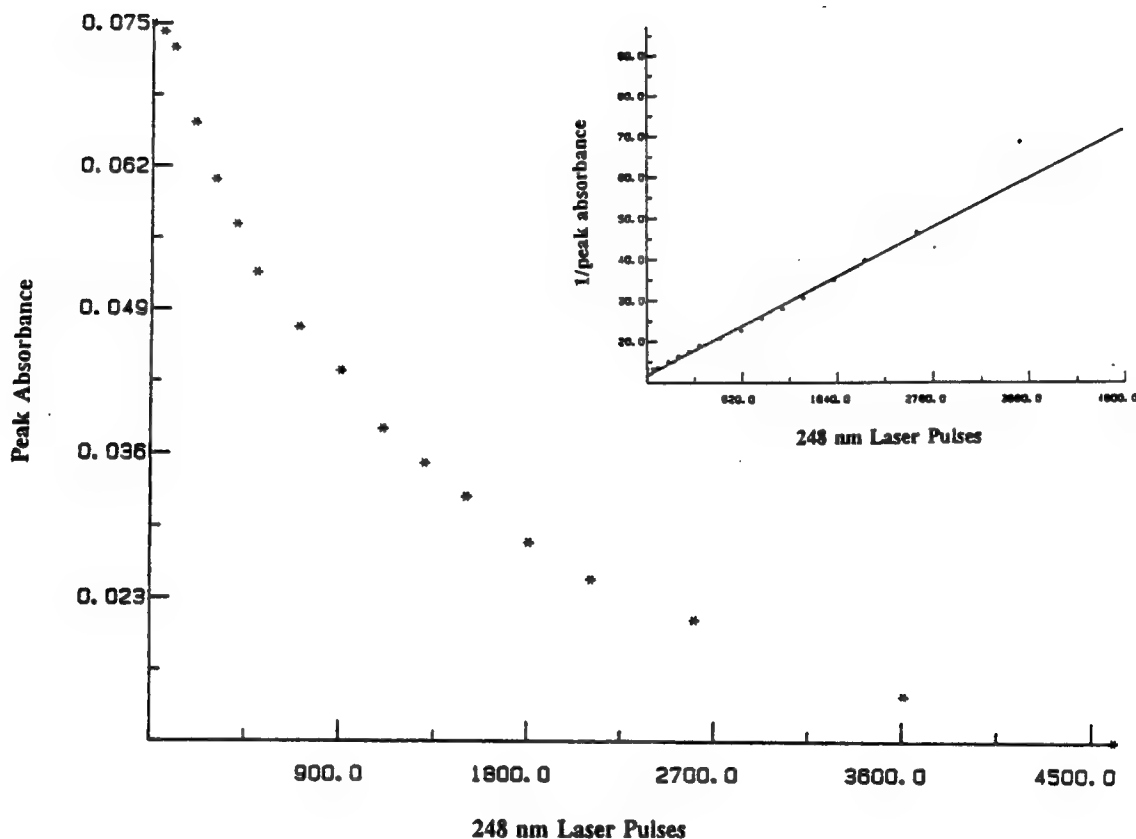
Figure 12

The peak absorbance of the R branch of the HBr monomer at 2508.4 cm^{-1} in a 1:400 HBr:Xe matrix is plotted versus the number of 248 nm laser pulses. A complete spectrum was recorded for each data point. The sample was photolyzed at 10 K using a laser fluence of 7.0 mJ/cm^2. $1/(I_{max}-I)$ versus the number of 248 nm laser pulses is shown as an insert.

Equation (52) involves the loss of two HBr molecules and the production of two Br atoms and is consistent with the observed bimolecular kinetics for both species in the matrices discussed in Figures 11-14. Reaction (52) leads to a differential rate expression of the form:

21

$$\frac{d[HBr]}{dn} = \frac{-d[Br]}{dn} = -k_1[HBr]^2 \qquad (53)$$

where n is the number of laser pulses. The reaction scheme implicit in equation 52 suggests there should be far fewer free H atoms generated than Br atoms since the H atoms would be expected to react with HBr to produce H_2. Consistent with this expectation the maximum concentration of stable H atoms created during the production/loss process of an ~ 1:800, HBr:Xe matrix is more than an order of magnitude less than the concentration of Br atoms produced.[3,7]
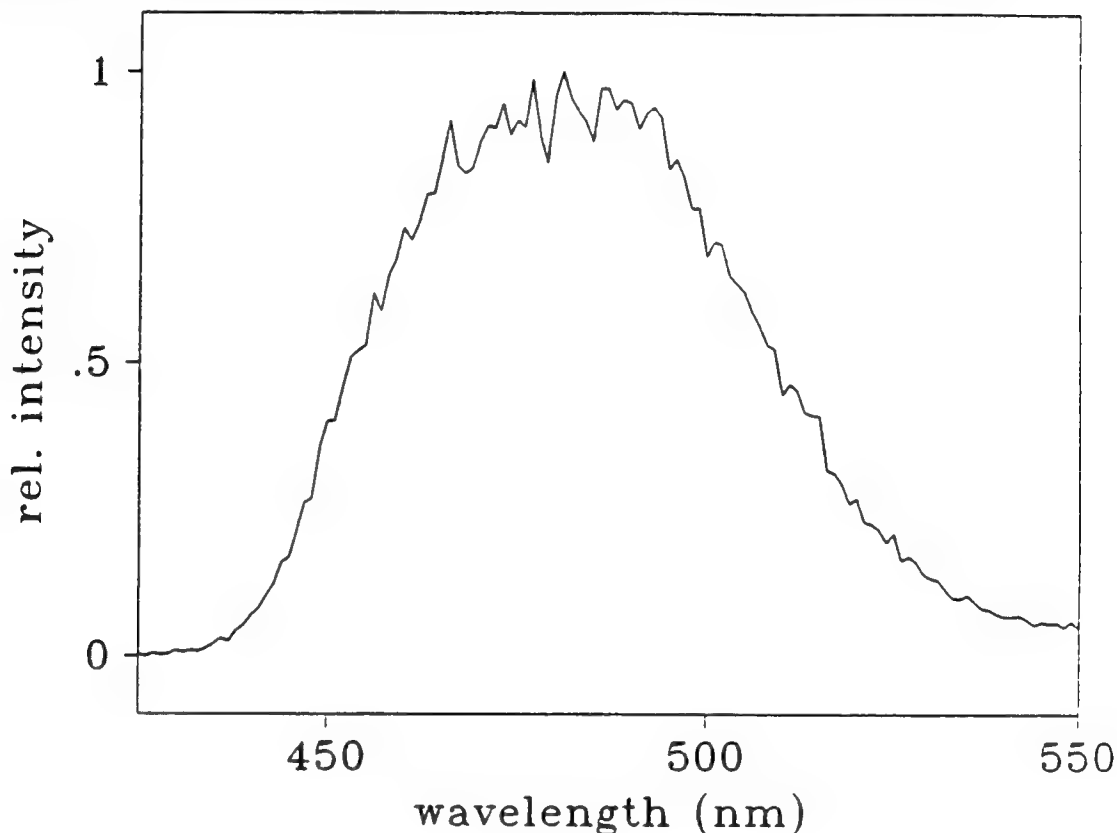
Figure 13

A Xe_2Br emission spectrum generated using 1.0 mJ/cm^2 308 nm laser pulse subsequent to ArF irradiation of a 1:800 HBr/Xe matrix at 10 K.

Though the overall reaction in equation (52) qualitatively accounts for the observed bimolecular behavior for the matrices in Figures 11-14, it does not explicitly provide a means to determine microscopic rate constants from experimental data nor does it directly provide a rationale for the observed change in order of the kinetics from second order to first order as the HBr concentration is decreased. To obtain this information it is necessary to formulate a mechanism delineating the elementary kinetic steps that are operative in this system.

22

$$HBr + h\nu_{193/248} \rightarrow H + Br \qquad k_\theta = I\sigma_{HBr/\lambda} \qquad (54)$$
$$H + HBr \rightarrow H_2 + Br \qquad k \qquad (55)$$
$$H + Br \rightarrow HBr \qquad k \qquad (56)$$
$$H + H \rightarrow H_2 \qquad k \qquad (57)$$
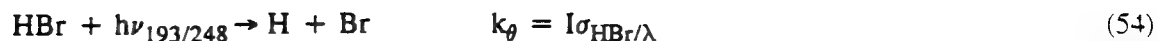
In this formulation I is the laser pulse intensity in photons/cm^2/sec and σ is the effective absorption cross-section in cm^2. As discussed previously in detail, σ can be written as $\sigma_1\phi_1$ where σ_1 is the intrinsic absorption cross-section and ϕ_1 is the cage exit probability.[1] As a first approximation, the rate constants, k for equations 55-57, are assumed to be the same since each reaction is expected to be limited by the mobility of the H atom reactant.
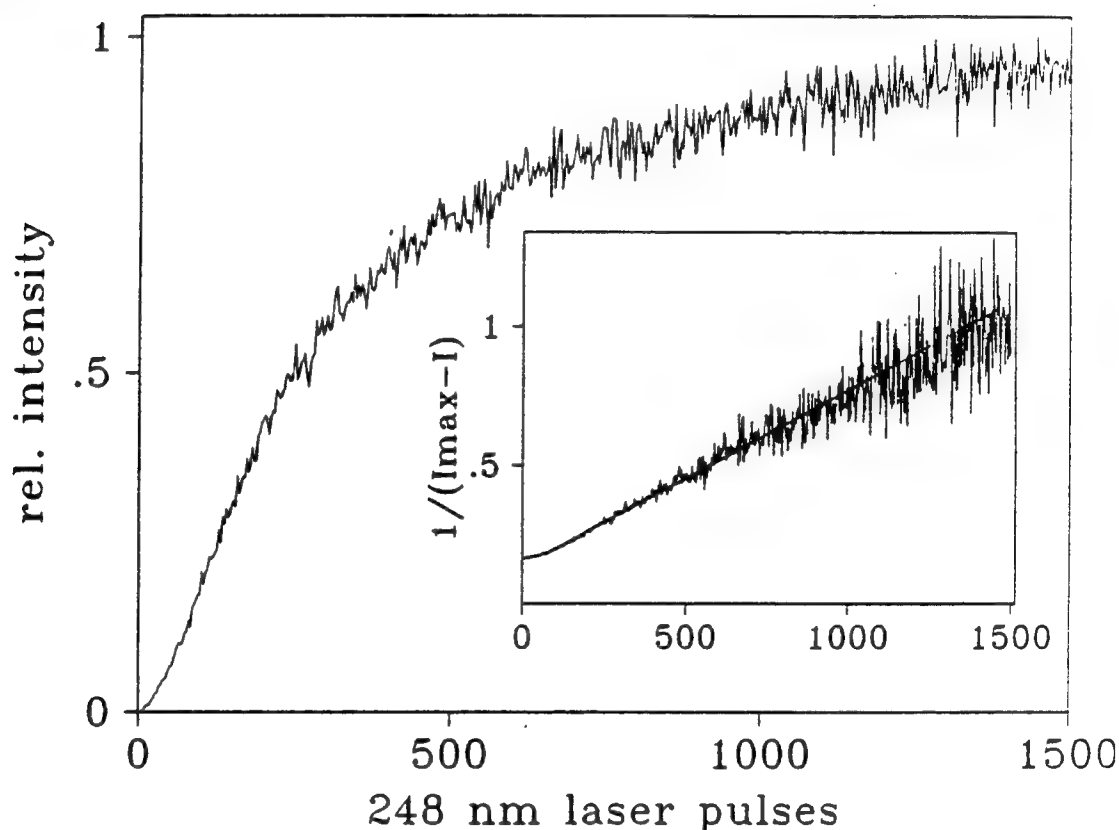
Figure 14

A plot of Xe$_2$Br emission as a function of laser pulses for 248 nm irradiation of a 1:400 HBr/Xe matrix at 10 K. The inset is a plot of I/I$_{max}$-I) vs. pulses.

Any such reaction mechanism must be consistent with the observed kinetics and therefore must involve stable Br atoms and HBr molecules as well as mobile H atoms. In the regime where second order kinetics are applicable, H atoms can be considered to be a transient species whose overall concentration does not vary significantly in time once an initial growth period has occurred.

This issue will be explored in more detail in a subsequent publication dealing with the details of H atom production and loss.[7] As such, equation 57, which involves the square of a small concentration, can be neglected. Given these assumptions, the following differential rate expression can be written

$$\frac{d[H]}{dn} = k_\theta[HBr] - k[H][HBr] - k[H][Br]$$ (58)

Under these conditions the application of the steady state approximation to the transient H atom species gives

$$[H]_{ss} = \frac{k_\theta[HBr]}{k([HBr] + [Br])}$$ (59)

using the Br atom mass balance

$$[Br] = [HBr]_0 - [HBr]$$ (60)

equation (59) can be rewritten as

$$[H]_{ss} = \frac{k_\theta[HBr]}{k[HBr]_0}$$ (61)

Using

$$\frac{d[HBr]}{dn} = -k_\theta[HBr] - k[H][HBr] + k[H][Br]$$ (62)

and the expression for $[H]_{ss}$ in eqn. 61 and [Br] in eqn. 60 gives:

$$\frac{d[HBr]}{dn} = \frac{-d[Br]}{dn} = \frac{-2k_\theta}{[HBr]_0}[HBr]^2$$ (63)

After integrating equation 63 over the number of laser pulses, the following expressions for the laser pulse dependance of the HBr and Br atom concentrations are obtained.

$$[HBr] = \frac{[HBr]_0}{1 + 2k_\theta n}$$ (64)

and

$$[Br] = [HBr]_0 - \frac{[HBr]_0}{1 + 2k_\theta n}$$ (65)

24

Equation 63 relates the phenomenological rate constant for the photolytic loss of HBr and the production of Br atoms to microscopic rate constants. It is essentially the effective photodissociation cross section for HBr weighted by the initial concentration of HBr, i.e.,

$$k = \frac{2I\sigma_{HBr/\lambda}}{[HBr]_0} \tag{66}$$

Therefore,

$$\sigma_{HBr/\lambda} = \frac{k[HBr]_0}{2I} \tag{67}$$

These equations immediately provide a method for computing the effective photodissociation cross-section for HBr in the matrix and demonstrates why the phenomenological rate constant for HBr loss and Br production should be equal at a given wavelength for a constant fluence photolysis pulse. Computing the effective photodissociation cross section of HBr from the observed bimolecular rate constants for HBr loss and Br atom production gives

$$\sigma_{HBr/193} = 2.9 \pm 0.3 \times 10^{-18} \text{ cm}^2$$
$$\sigma_{Br/193} = 2.1 \pm 0.2 \pm 10^{-18} \text{ cm}^2$$
$$\sigma_{HBr/248} = 4.8 \pm 0.5 \times 10^{-19} \text{ cm}^2$$
$$\sigma_{Br/248} = 4.9 \pm 0.5 \pm 10^{-19} \text{ cm}^2$$

The values of σ obtained for 193 nm photolysis are close to the gas phase photodissociation cross section at 193 nm of $\sigma_{HBr/193/gas} = 1.79 \times 10^{-18} \text{ cm}^2$.[14] The gas phase cross-section at 248 nm is at least an order of magnitude smaller than the cross-section at 193 nm.[14] Thus the value of the cross-section for 248 nm photolysis in the matrix is at least a factor of two larger than the corresponding gas phase cross-section and the 248 nm cross-section is slightly larger than the measured gas phase value. A modest enhancement in these cross-sections due to the dielectric constant of the matrix is expected. However, enhancements of photolysis cross-sections in a matrix environment have been observed before, especially at the tail of an absorption profile where small shifts in the energies of different electronic states can result in significant changes in the observed cross-section.[34] These results imply that the cage exit probability ϕ is near unity for H atoms produced on 193 nm photolysis of HBr and is also likely to be large for 248 nm photolysis.

Equations (54-57) also provide insight into the rationale for a transition from second to first order kinetics as a function of changing concentration. The observation of second order kinetics implies that reaction (55) occurs with high efficiency and consumes most of the H atoms that are generated in the initial photolysis step (54). This will only occur when the range of H atom motion is comparable to the distance between reaction centers. This distance will increase with increasing dilution and eventually the range of motion will be less than the mean distance between reaction centers and reaction (55) will not be efficient. In the limit where the mean distance greatly exceeds the range of H atom motion reaction (55) will not occur to any significant extent and HBr loss is expected to exhibit first order behavior as is growth of Br atoms and H atoms.

The predictions of this simple model are realized on examination of the data. As shown in Figure 15, for 248 nm photolysis of a dilute matrix, growth of Br exhibits first order kinetics.

25

At these dilutions it was not possible to also monitor the loss of HBr. Similar changes in the kinetics of atom products are observed for H atoms.[25] The fact that the dilutions at which this change in order of the kinetic processes occurs is significantly different for the two wavelengths provides insights into the dynamics of H atom motion discussed below and in reference 7.
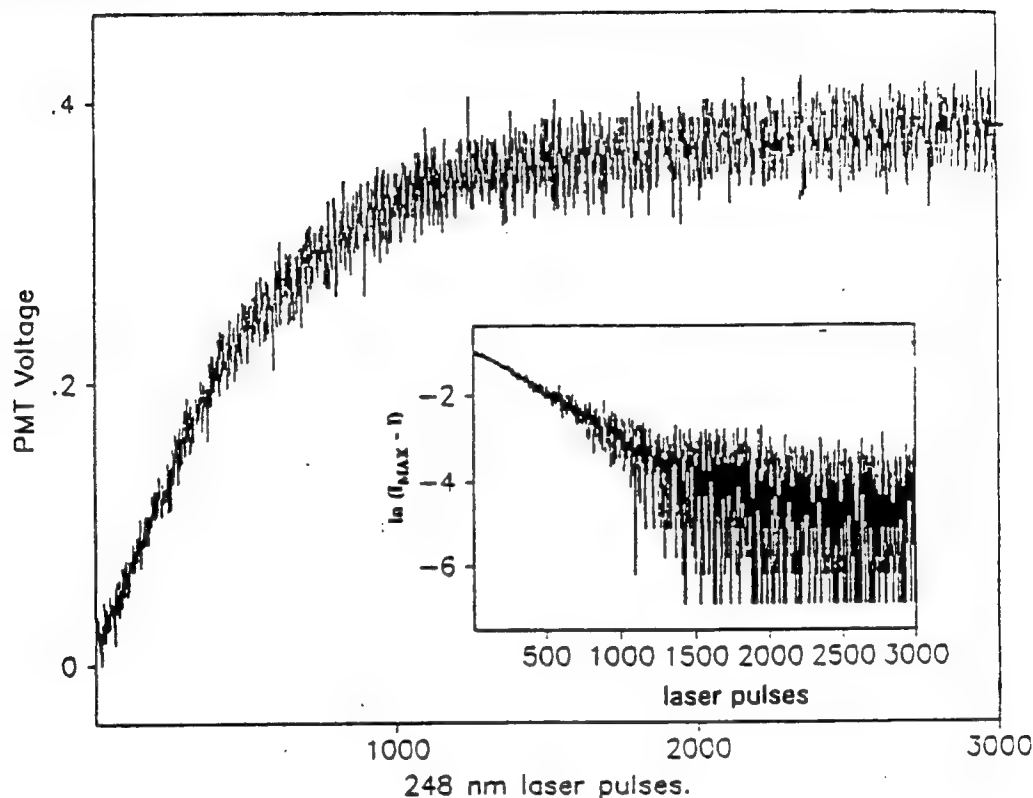
H Atom Dynamics

Figure 15

A plot of Xe_2Br emission vs. 248 nm laser pulses for a matrix with composition of ~1:100,000. The inset is a plot of $\ln(I_{max}-I)$ vs. laser pulses.

The qualitative similarity of the H atom photoproduction curves at 193 and 248 nm indicate that dissociative relaxation of Xe_2H exciplexes cannot be the major factor in H atom motion since these exciplexes do not absorb at 248 nm. Thus the major factor in exciplex motion is simply a result of the energy channeled into the H atom in the dissociation of HBr. The quantitative difference in the shape of the 248 vs 193 nm photoproduction curves, particularly with respect to the rate of depletion of the "plateau" level of H atoms established at steady state, is due to dissociative relaxation of exciplexes which can occur at 193 nm (see Figure 16). This is born out by a detailed analysis of these curves which is presented in reference 7.
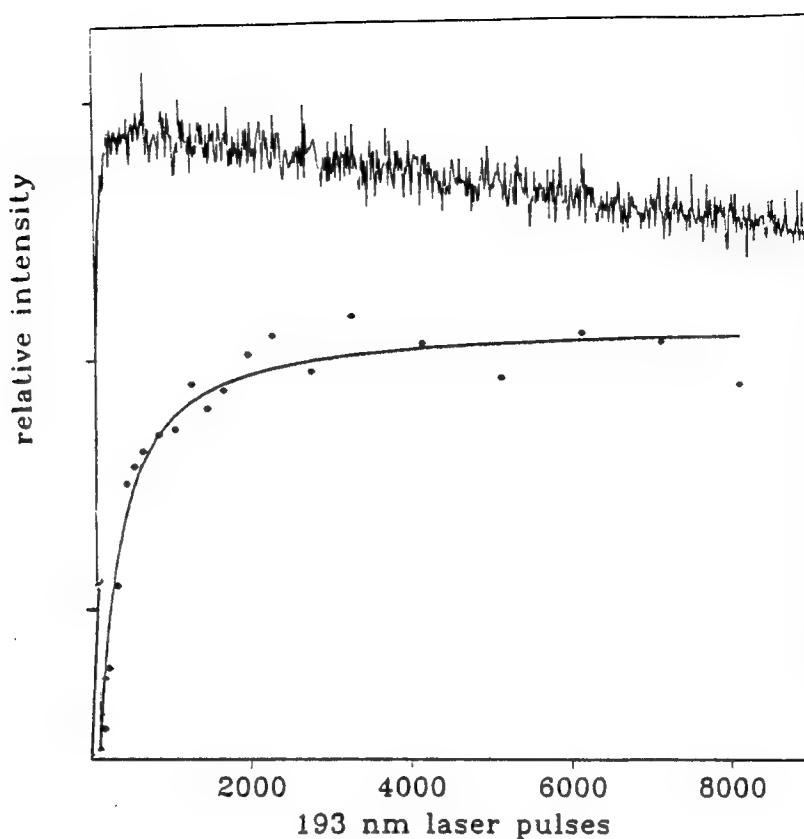
26

Figure 16

H atom production curves from a 1:800 HBr:Xe matrix (upper line). Also pictured is an H atom production curve for a 1:400 HBr:Xe matrix on 248 nm photolysis. The Xe$_2$H exciplexes were excited using 193 nm pulses of greatly reduced intensity. The finite number of probe pulses accounts for the difference between the data point density for this curve versus the curve for 193 nm photolysis.

As with Br atoms there is a transition region for the production of H atoms which is indicative of the point at which the range of H atom motion exceeds the average distance between HBr molecules. For lower concentrations the production of H atoms is first order: indicative of single photon photodissociation of HBr. For higher concentrations the production of H atoms has a more complex form due to a competition between production and reaction with HBr, H atoms and Br. In this regime the steady state H atom concentration is greatly reduced relative to the steady state Br atom concentration due to reactive loss. As seen in Figure 17, H atom production is mostly first order for a 1:100,000 HBr:Xe matrix. For a 1:10,000 HBr:Xe matrix the kinetics clearly indicate a competition between first order production and reaction.

These curves indicate that the range of H atom motion for 193 nm photolysis of HBr is comparable to the average internuclear spacing of HBr molecules in a 1:10,000 matrix. This is on the order of 100 Å. Whether the reactive loss of H atoms that occurs in a 1:100,000 matrix is due to the tail of the H atom kinetic energy distribution or to reactions of HBr molecules that are closer than statistical awaits further study on this system.
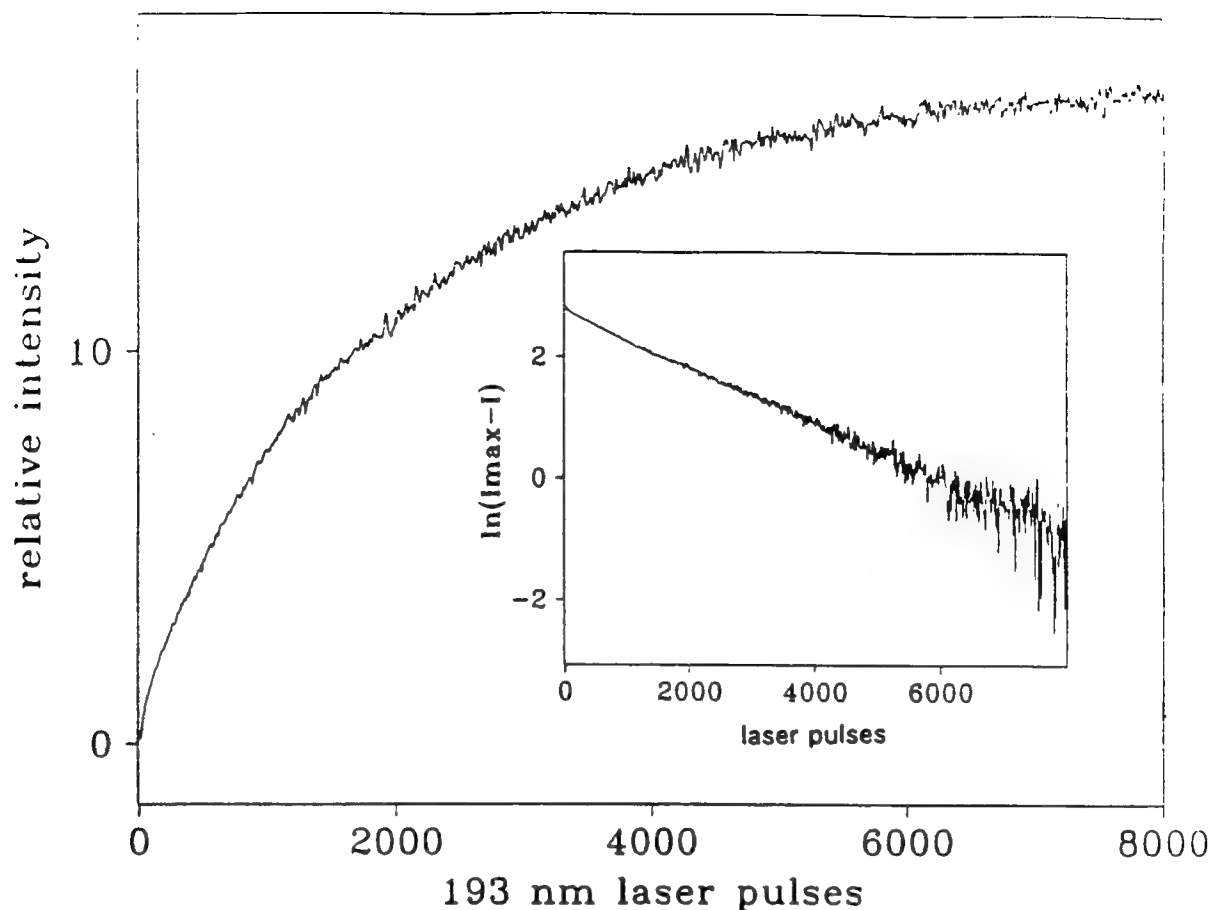
27

Figure 17

H atom production curve for a matrix estimated to have a mole ratio of 1:100,000. The inset is a plot of the log (exciplex emission intensity) versus number of laser shots.

H Atom Diffusion

Figure 18 is a comparison of the 40 K loss rates for the two different deposition temperatures. It demonstrates the strong dependance of the thermally induced loss rate on the degree of crystallinity of the matrices. The 5 fold increase in the 40 K loss rate for matrices deposited at 10 K relative to 28 K establishes the fact that the reaction rate is not governed by a chemical reaction activation barrier but is limited by thermal mobility of the atoms. Though the thermal mobility of atoms in rare gas solids may not be governed by the same dynamics as diffusive behavior in solutions, such mobility limited reactions have typically been treated using the formalism of diffusion controlled processes.[15]

A precise diffusion limited reaction rate constant cannot be determined until the details of the reactive loss mechanism are known. It is however possible to compute an approximate value for the diffusion coefficient of H atoms from the observed reaction rate constants, k_{obs}, of the bimolecular plots. Since the 40 K reaction rates are diffusion limited the observed rate constant has the following form for reaction 68,

28

$$k_{obs} = 4\pi r_{HH} D \qquad (68)$$

Where $r_{HH} = 0.7046$ Å, the bond distance for H_2 and D (cm^2/s) is the diffusion coefficient. Once the Xe_2H emission intensity measurements are converted to H atom concentration the data can be plotted using the following equation for bimolecular loss kinetics:
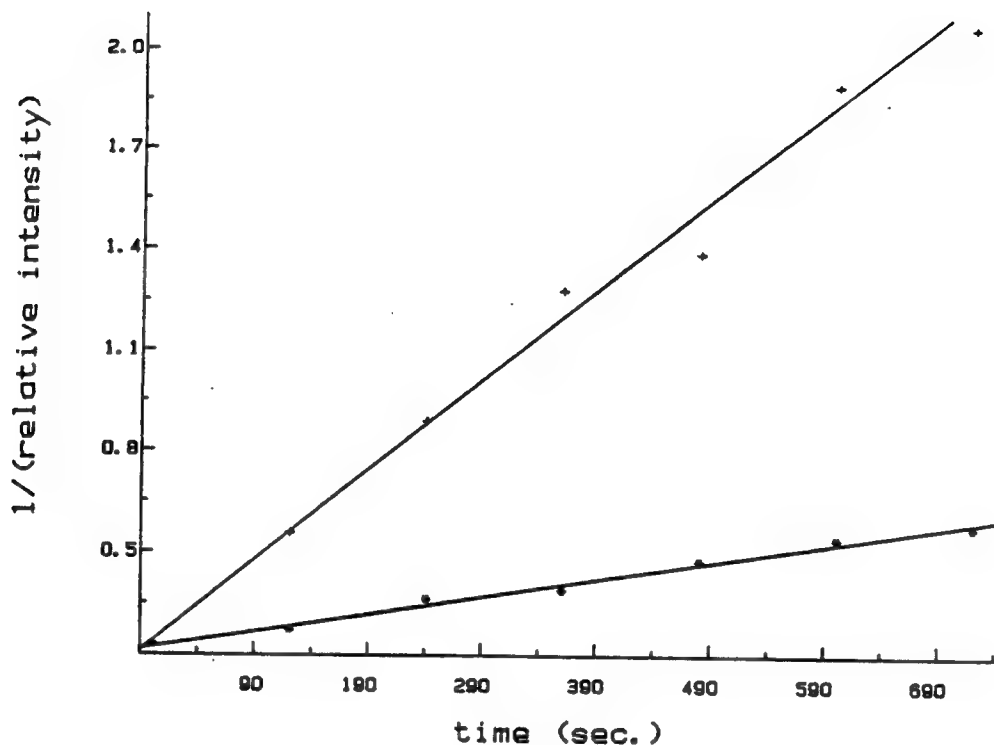
Figure 18

A plot of the reciprocal of the Xe_2H emission intensity versus time. The Xe_2H emission intensity was recorded at 250 nm and 40 K using laser pulses having a fluence of 1 mg/cm^2 at 193 nm. The upper line is for a matrix deposited at 10 K while the lower line is for a matrix deposited at 28 K.

$$\frac{1}{C_H} = \frac{1}{C_{H_0}} + k_{obs}t \qquad (69)$$

Where C_H is the H atom concentration at time t and C_{H_0} is the initial H atom concentration. Computing best fits to the 40 K bimolecular plots of Figure 18, diffusion coefficients of $D_{28K} = 4.8 \times 10^{-15}$ cm^2/s and $D_{10K} = 2.5 \times 10^{-14}$ cm^2/s are derived for matrices deposited at 28 and 10 K, respectively. The experimental values for k_{obs} are reproducible to within 10 %. The largest source of error in the calculation of the diffusion coefficients is the estimation of the initial H atom concentrations.

29

The 40 K diffusion coefficients for H atoms determined for the two different deposition temperatures show the direct link between diffusive motion and matrix morphology. Though to our knowledge this is the first report of the effect of matrix morphology on mobilities, several recent experimental and theoretical investigations have indicated the importance of Rg matrix morphology on such things a photodissociation cross sections and reaction product distributions.[35] We believe that deposition near the annealing temperature of Xe will have an even more drastic effect on the diffusion rate as compared to the present study. Such control over the matrix morphology has been demonstrated to effect the rate of diffusion limited reactions and may represent a general approach to control the rate of reactions in the solid state.

Diffusion of HBr

Though we have not performed a detailed study in an attempt to provide an exact correspondence between the features identified in lighter rare gas matrices and those observed in xenon, it is clear that there is a qualitative correspondence between features that are observed both before and after annealing.[36] Thus we can confidently assign features observed to grow in on annealing of HBr doped xenon matrices at lower frequency than parent to dimers and multimers. These lower frequency features are already prominent, prior to annealing, in the matrix deposited at 45 K. Corresponding absorptions grow in or become more intense on annealing of the sample deposited at 28 K. Table 2 presents the positions of the absorptions observed in this study.

Table 2. HBr Frequencies (cm^{-1})

R(0)	2530.9
Q	2520.1
P(1)	2508.7
Dimer	2492.3
and	2474.5
Multimer	2468.7
	2455.7

Interestingly, as seen in Fig. 19, there is very significant growth in the intensity of these dimers and multimer peaks on annealing of the matrix deposited at 28 K but little if any growth of these peaks on annealing of the sample deposited at 45 K despite the fact that the sample deposited at 45 K is annealed for *10 minutes longer* than the sample deposited at 28 K. As expected, growth of the dimer and multimer peaks is associated with a loss of intensity of the parent peak. In fact virtually complete mass balance is achieved if it is assumed that $(HBr)_n$ species with larger n's are progressively red shifted and these species have integrated absorption coefficients that scale with n relative to HBr.

This data implies that the mobility of HBr in a xenon matrix can be strongly influence by depositions conditions. A similar observation was made regarding the effect of mobility on H atoms in xenon.[3] For the H atom system this observation was rationalized as resulting from a change in the morphology of the matrix as a function of deposition temperature. This morphology
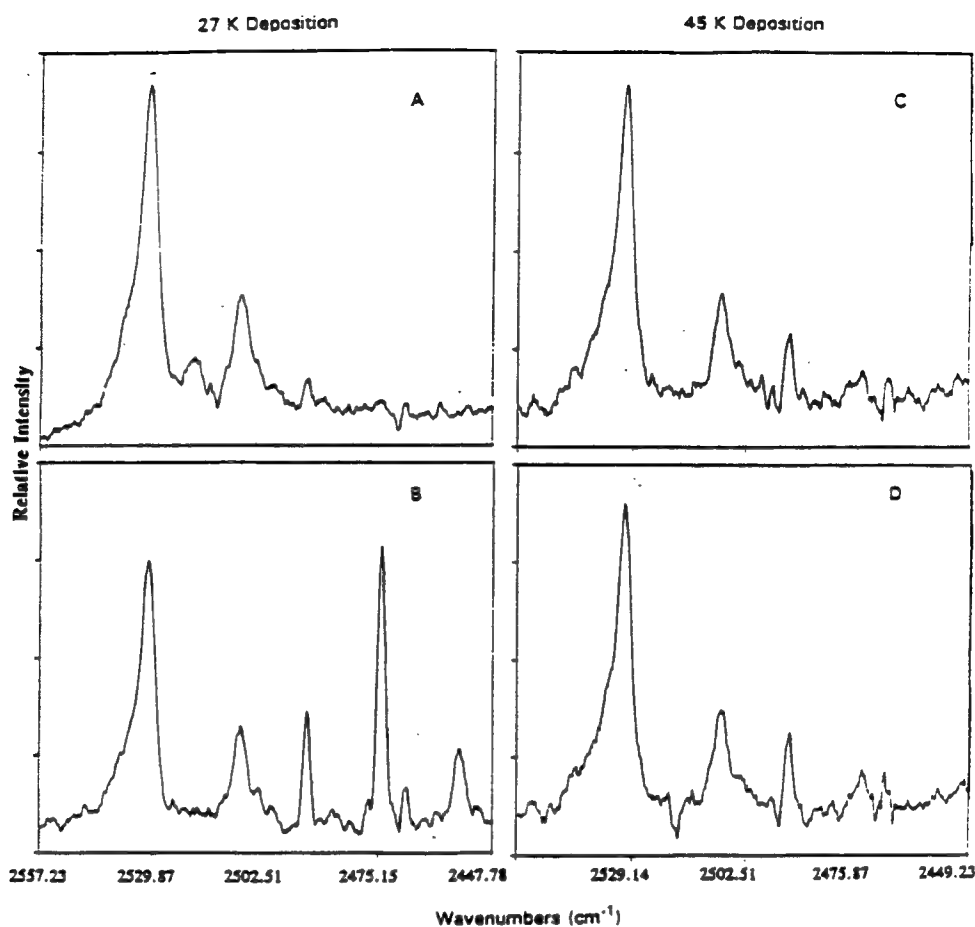
Figure 19

Spectra of a 1:1600 HBr:Xe matrix. Panel A is a spectrum of a matrix deposited at 28 K with panel B a spectrum of the same matrix following annealing at 50 K for 30 minutes. Panel C is a spectrum of a matrix deposited at 45 K with panel D a spectrum of the same matrix following annealing at 50 K for 40 minutes. All spectra were recorded at 10 K.

change in turn can effect the mobility of a dopant. This can occur since a Xe matrix is composed of an ensemble of face centered cubic microcrystalline grains surrounded by disordered regions called grain boundaries. The much larger increase in the percentage of dimer and multimers that occurs as a result of 50 K annealing of the matrix deposited at 28 K versus the matrix deposited at 45 K provides evidence that the percentage of grain boundary relative to microcrystals is larger in matrices deposited at 28 K than at 45 K. This is consistent with the experimental observation of a greater degree of visible light scattering observed from matrices deposited at 28 K as compared to 45 K. The increased light scattering is likely due to an increase in sample density fluctuations on the length scale of visible light. The potential energy surface of the grain boundary regions is such that the barrier height to thermally induced motion is effectively reduced compared

31

to more crystalline regions. This further implies that the mechanism for HBr diffusion at 50 K is defect driven. The self diffusion rate for Xe at 50 K can be approximated by extrapolating the results a recent study to 50 K yielding a diffusion coefficient of roughly 10^{-38} cm^2/s.[37] This would result in no observable diffusion of HBr on the timescale of annealing. While the extrapolation is extreme this indicates the Xe self diffusion coefficient should be many orders of magnitude smaller than that observed for HBr molecules. This further suggests that HBr thermal diffusion at 50 K follows either a defect mediated interstitial or substitutional mechanism.

C Atom Generation

Photolysis of C_3O_2 is a potential source of C atoms via a sequential two photon process which also generates CO. C_3O_2 was synthesized and the significant CO_2 impurity was removed by successive distillations. The photodissociation of C_3O_2 and the wavelength dependance of the production of various electronic states of C_2O was monitored by infrared emission from CO. Though results in this area should be considered as preliminary, the wavelength dependance we have obtained to date are consistent with the interpretation of this problem by Bayes.[28]

O Atom Storage in Solid O_2

We have obtained data that suggest that it is possible to store O atoms in solid O_2. O atom storage in this environment is dependent on matrix preparation. The relevant data is contained in Figure 20 which displays the IR spectra and emission spectra obtained following 193 nm irradiation of two matrices of the same initial composition. The matrix in the bottom row was annealed while the one in the top row was not. Note that for the matrix in the top column there is growth of a significant O_3 peak following UV irradiation and no significant XeO emission as a result of averaging 3000 UV pulses which, as seen in the IR spectra, is sufficient to photolyze virtually all of the N_2O that was initially present. This behavior suggests that the O atoms generated by photolysis of N_2O reacted with the O_2 in the matrix to form O_3. However, the behavior of the matrix that is annealed prior to photolysis is very different and very intriguing. For this matrix there is a large XeO emission signal after only 50 pulses and **very little growth of O_3** after photolysis of a significant fraction of the N_2O present. This behavior indicates that annealing "protects" O atoms and inhibits their reaction with the O_2 molecules in the matrix. Annealing is accompanied by a large shift in the frequency of the N_2O asymmetric stretching mode. We believe that the shift and the inhibition of the reaction of O with O_2 are manifestations of preferential clustering of Xe atoms around N_2O molecules which serves to "protect" the O atoms from reaction with O_2. Formation of a "xenon cluster" around an N_2O would give an O atom surrounded by xenon which is compatible with the observation of the same emission spectra for XeO complexes in this matrix as in a normal xenon matrix. This is very interesting and unusual behavior, and suggests some strategies for isolating other reactive species. Future work on this system will involve using a quartz microbalance to quantify potential loss of matrix material during annealing.

32
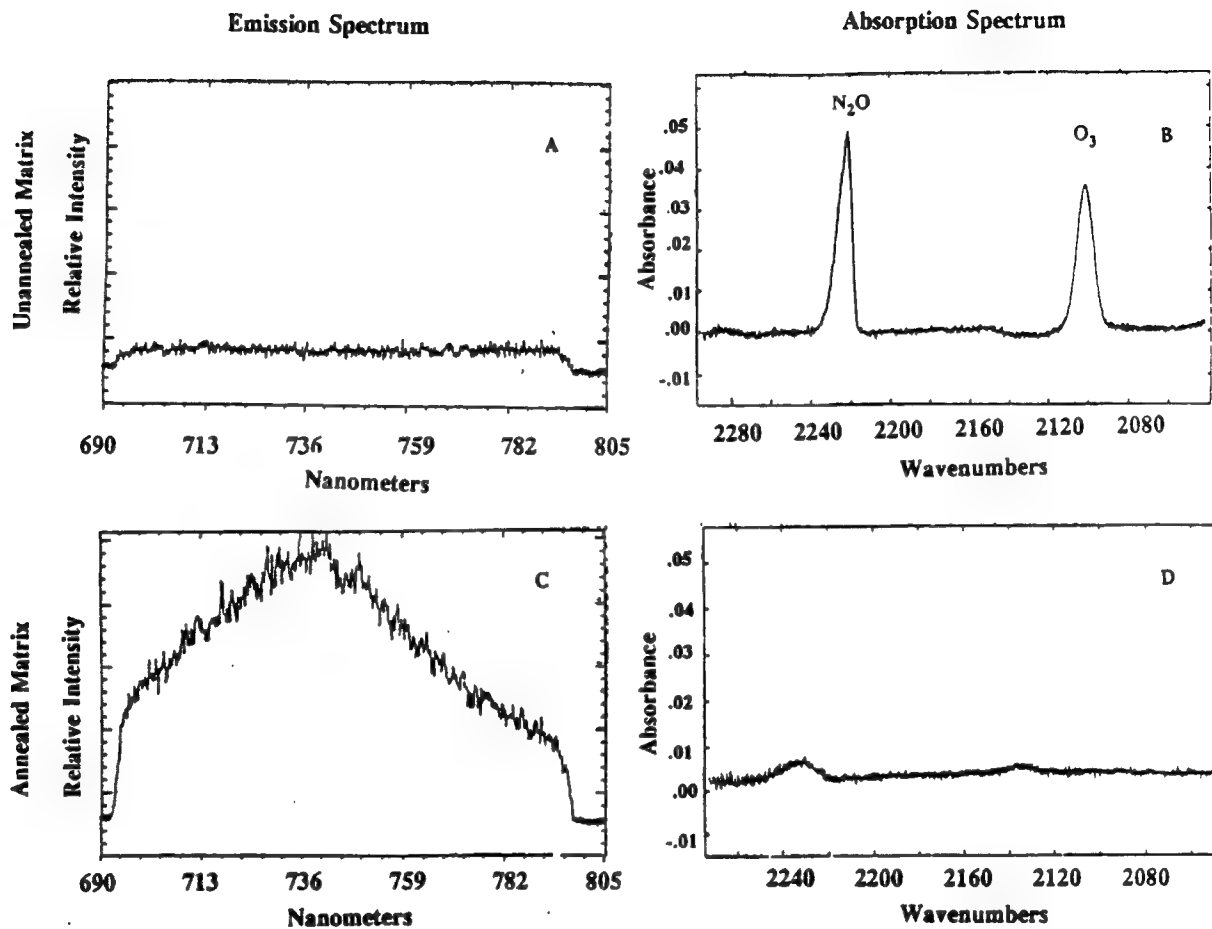
Figure 20

Data from a 1:32:348 N_2O:Xe:O_2 matrix. Data is shown for an unannealed matrix (A & B) deposited at 10 K with emission spectra in panel A obtained by averaging 6000 ArF laser pulses and infrared spectra (B) following 3000 laser pulses. Panel C is emission spectra recorded as a result of 50 ArF laser pulses for a matrix that was deposited at 10K and then annealed before recording the spectrum produced as a result of photolysis at 10K. The infrared spectrum in panel D was recorded for the matrix in panel C after 3000 photolysis pulses.

CONCLUSIONS

The 193 nm photolysis of matrix isolated N_2O generates $O(^1D)$ atoms which are rapidly relaxed to $O(^3P)$ in a xenon matrix. The time evolution of the photolytically generated O atoms can be described by a mechanism in which the O atom concentration is governed by a competition between the rates of photoproduction and photoinduced O atom loss. Photoinduced mobility occurs as a result of 193 nm excitation of xenon oxide charge transfer states which relax to exciplex states and can subsequently dissociate with the release of significant kinetic energy. The majority of this energy is channeled into O atom translational motion. The O atom photoproduction rate is relatively insensitive to temperature while the photoinduced mobility of O atoms, which can lead to O atom recombination is very temperature sensitive. The cross-section for dissociation of N_2O in Xe is comparable to that found in the gas phase. This cross section decreases approximately 10% for every 10 K increase in temperature. A decrease in temperature results in the production of a larger concentration of O atoms due to the loss process being less efficient at low temperature. O atom loss at high temperature (42 K) is found to be bimolecular but there may be an initial first-order contribution to the decay. The kinetic model developed predicts this behavior and demonstrates that when the reaction of mobile O atoms dominates translational quenching, the loss process is expected to become first-order. O atom motion on the order of 100 Å is seen at higher temperatures.

The photoproduction and subsequent chemical reactions of O atoms in N_2O doped Xe and N_2 matrices have been studied. In Xe matrices, O atom photoproduction was studied as a function of the N_2O dopant concentration. An O atom concentration of at least 32 mmolar can be "stored" in this system. The kinetic model discussed above accurately predicts the maximum concentration of atomic oxygen in dilute and moderately doped matrices but severely deviates from the data obtained in a highly doped matrix. This deviation is a result of reactions of O atoms produced in aggregates of N_2O, which form in matrices doped with a large amount of N_2O, and which are not included in the previously developed kinetic model for O atom production. Inclusion of additional reactive pathways leads to better quantitative agreement with the data but there are still quantitative differences between the data and the model. We believe this continued lack of agreement is due to attempts to model inhomogeneous reacting systems using homogeneous kinetic equations.

The growth of reaction products upon the photolysis of a neat N_2O matrix and N_2 matrices doped with isotopically labelled N_2O demonstrate the occurrence of O atom chemistry in these systems. The nature of these reactions points to $O(^1D)$ as the reactive species. These reactions are likely to occur between photolytically generated $O(^1D)$ atoms and surrounding N_2O molecules. On photolysis of $^{15}N^{14}NO$ in N_2, $^{14}N_2O$ is formed in high yield. O atom reactions with N_2O were not observed in dilute Xe matrices which is consistent with quenching of $O(^1D)$ atoms before they can travel sufficient distances to react with N_2O.

Matrix morphology influences N_2O photodissociation efficiency in Xe matrices with larger cross-sections in matrices deposited at lower temperatures which yields more amorphous matrices. There is also evidence for enhanced in-cage recombination of N_2 with O in more crystalline matrices.

The UV photodissociation of HBr in xenon results in the production of translationally excited H atoms. The excitation process is dominated by the disposition of the energy of the photolytic radiation into the translational degrees of freedom of the photoproducts. This process is analogous to that used to photolytically produce translationally hot H atoms in the gas phase.

These translationally excited H atoms are mobile and readily react with neighboring HBr molecules in the solid Xe samples. When the average spacing between HBr molecules is small compared to the mean distance traveled by an H atom, a large fraction of H atoms react with HBr molecules leading to photolytic loss of HBr and the photolytic production of Br atoms which are second order in the HBr concentration even though HBr is being dissociated by a single photon process. The phenomenological second order rate constant for this processes depend only on the laser fluence, the photodissociation cross section of HBr, and the initial HBr concentration. The photodissociation cross section for 193 nm photolysis of HBr is close to that measured for the gas phase and has only a small temperature dependance consistent with a modest temperature dependance for the HBr absorption cross-section in xenon matrices. The cross-section for 248 nm photolysis is enhanced relative to the gas phase.

At higher dilutions, where the average distance between HBr molecules is large compared to the mean distance traveled by an H atom, reactions between H atoms and HBr molecules are unlikely and loss of HBr follows first order kinetics as does production of Br atoms. The concentration at which the transition between first order and second order loss of HBr occurs is dependant on the energy deposited in the HBr molecule and thus on the wavelength of the photolytic radiation. For 193 nm photolysis the mean distance traveled by H atoms is on the order of 100 Å at 10 K.

All of the reported behavior is dominated by single photon dissociation of HBr followed by a competition between relaxation of H atom translational energy and reaction of the H atom. H atom mobility as a result of dissociative relaxation of Xe_2H exciplexes is present but is a less important process. It leads to reactive loss of H atoms after a majority of the HBr has been photolyzed.

The Br atom co-photofragment is thermally stable and does not exhibit significant mobility as a result of the initial photodissociation process or dissociative relaxation of Xe_2Br exciplexes at least for temperature below 40 K. This is presumably due to the mass and size of the Br atom and the dynamical constraints which channel far less energy into Br than the H atom co-fragment.

At 10 K, the H atom concentration produced by 193 nm photolysis of HBr, remains unchanged over the course of five days. At 40 K atom loss occurs on a timescale of minutes and is sensitive to matrix preparation. At 40 K diffusion coefficients for H atom motion have been estimated as 4.8×10^{-15} cm^2/s and 2.5×10^{-14} cm^2/s for xenon matrices deposited at 28 and 10K respectively. The difference in morphology of the xenon matrices deposited at 10 and 28 K leads to these differences in diffusion coefficients. This difference implies that H atom motion in these systems is defect driven.

Similar behavior is observed for the diffusion of HBr in xenon matrices. Though more dimer and multimer formation is observed subsequent to higher temperature deposition, less formation of these species is observed on annealing of matrices deposited at higher temperatures. This result can be correlated with the greater degree of crystallinity obtained for higher temperature deposition. These results also imply that better isolated, more thermally stable *monomer* species are likely to be obtained by higher temperature as opposed to lower temperature deposition since higher temperature deposition favors the production of more "crystalline" lattices.

We have presented evidence that suggests that O atoms can be isolated in solid O_2 but that isolation requires the formation of a protective cluster of molecules around the O atom to inhibit its reaction with the solid O_2 host.

It seems appropriate to include a few paragraphs on the implications of these studies for the storage of reactive species in cryogenic media. It is clear that both O atoms and H atoms can be stabilized at chemically significant concentrations in rare gas solids at 10 K for a period that exceeds days. However, it is also clear that there are impediments to producing concentrations of these species in the percent range. Principally, reactions must be avoided. These reactions can be with other reactive species or with parent. For stored atoms reactions will lead to atom recombination. For a species such as C this will produce C_2 which itself is a reactive species. However, recombination reactions are clearly undesirable for O and H atoms. Such reactions can be minimized by decreasing the mobility of the reactive species. Both photoinduced and thermal mobilities must be considered. Though our data base is not extensive, both systems that have been studied in detail do lead to the same conclusions.

Mobility can be minimized by operating at a low temperature in a more crystalline environment. Photoinduced mobility can be avoided by photolysis of the parent species at a wavelength that is not absorbed by potential exciplexes. Longer wavelength photolysis will minimize the energy that is available for disposal into translational degrees of freedom of the products. A light co-fragment will also reduce available energy in the species of interest. Reactions with parent can be minimized if it requires a spin disallowed process. There is no evidence of reaction of $O(^3P)$ atoms with N_2O while $O(^1D)$ atoms react. Our work on the storage of atomic O in solid O_2 indicates that a possible strategy for isolation of reactive species in a potentially reactive matrix involves the formation of a "protective shell" of non-reactive species around the reactive dopant. In the aforementioned system this may occur by clustering of Xe and/or N_2O molecules around an O atom. However, it is possible to imagine a cryogenic system made up of intentionally synthesized clusters of a reactive species surround by an unreactive protective shell. In addition the role of collective effects in low temperature solids has not been extensively explored. These may provide a barrier to reaction that does not have a counterpart for gas phase systems. As a final comment we note that the >32 mmole concentration of O atoms that we have stored in Xe is to our knowledge the highest reported concentration of stored atoms or reactive radicals that has been achieved to date. We are confident that this concentration could be significantly increased as a result of further work on this system.

REFERENCES

1. E. T. Ryan and E. Weitz, *J. Chem. Phys.* **99**, 1004 (1993).
2. E. T. Ryan and E. Weitz, *J. Chem. Phys.* **99**, 8028 (1993).
3. D. LaBrake and E. Weitz, *Chem. Phys. Letters* **211**, 430 (1993).
4. A. Moustakas and E. Weitz, *J. Chem. Phys.* **98**, 6947 (1993).
5. E. T. Ryan and E. Weitz, *Chem. Phys.*, in press.
6. D. LaBrake, E. T. Ryan and E. Weitz, to be published.
7. D. LaBrake, E. T. Ryan and E. Weitz, to be published.
8. D. H. Fairbrother, D. LaBrake and E. Weitz, to be published.
9. M. E. Jacox, in *Chemistry and Physics of Matrix-Isolated Species*, edited by L. E. Andrews and M. Moskovits (Elsevier, Amsterdam, 1989).
10. V. E. Bondybey and L. E. Brus, *J. Chem. Phys.* **62**, 620 (1975); V. E. Bondybey and C. Fletcher, *ibid.* **64**, 3615 (1976); L. E. Brus and V. E. Bondybey, *ibid.* **65**, 71 (1976); V.

E. Bondybey, S. S. Bearder, and C. Fletcher, *ibid.* **64** 5243 (1976); V. E. Bondybey and L. E. Brus, *Adv. Chem. Phys.* **41**, 269 (1980).

11. H. Kunz, J. G. McCaffrey, R. Schriever, and N. Schwentner, *J. Chem. Phys.* **94**, 1039 (1991).
12. J. G. McCaffrey, H. Kunz, and N. Schwentner, *J. Chem. Phys.* **96**, 2825 (1992).
13. (a) M. E. Fajardo and V. A. Apkarian, *J. Chem. Phys.* **85**, 5660 (1986); (b) J. Feld, H. Kunttu, and V. A. Apkarian, *ibid.* **93**, 1009 (1990); (c) A. I. Katz and V. A. Apkarian, *J. Phys. Chem.* **94**, 6671 (1990).
14. A. Plonka, *Lecture Notes in Chemistry*, Vol. 40 (Springer, Berlin, 1980).
15. H. Krueger and E. Weitz, *J. Chem. Phys.* **96**, 2846 (1992).
16. H. Krueger and E. Weitz, *Proceeding of High Energy Density Matter Conference, Albuquerque, NM, February 1991*, edited by M. E. Cordonnier, Air Force Report No. PL-CP-91-3003.
17. A. V. Danilychev and V. A. Apkarian, *J. Chem. Phys.* **99**, 8617 (1993).
18. A. V. Danilychev and V. A. Apkarian, *J. Chem. Phys.* **100**, 5556 (1994).
19. H. Okabe, *Photochemistry of Small Molecules* (Wiley, New York, 1978).
20. T. Miyazaki, N. Iwata, K. Lee and K. Fueki, *J. Phys. Chem.* **93**, 3352 (1989).
21. H. Kung, J. G. McCaffrey, M. Chergui, R. Schriever, Ö. Ünal, V. Stepaneko and N. Schwentner, *J. Chem. Phys.* **95**, 1446 (1991); M. Kraas and P. Gürtler, *Chem. Phys. Letters* **183**, 264 (1991); M. Creuzburg and F. Wittl, *J. Mol. Struct.* **222**, 127 (1990).
22. G. W. Flynn and R. E. Weston, Jr., *Ann. Rev. Phys. Chem.* **37**, 551 (1986).
23. Xe_2Br
24. M. E. Fajardo and V. A. Apkarian, *J. Chem. Phys.* **89**, 4124 (1988).
25. J. Feld, H. Kunttu, and V. A. Apkarian, *J. Chem. Phys.* **93**, 1009 (1990).
26. See reference 19 in reference 2 for a discussion of the limitations of this assumption.
27. O. Kajimoto and R. J. Cvetanovic, *J. Chem. Phys.* **64**, 1005 (1976); W. DeMore and O. F. Raper, *J. Chem. Phys.* **37**, 2048 (1962); W. B. DeMore and N. Davidson, *J. Am. Chem. Soc.* **81**, 5869 (1959).
28. A. V. Benderskii and C. A. Wight, *Chem. Phys.*, **188** xxx (1994).
29. J. A. Davidson, C. J. Howard, H. I. Schiff and F. C. Fehsenfeld, *J. Chem. Phys.* **70**, 1697 (1978); H. N. Volltraner, W. Felder, R. J. Pirkle and A. Fontijn, *J. Photochem.* **11**, 173 (1979); J. R. Sodeau and R. Withnall, *J. Phys. Chem.* **89**, 4484 (1985); W. A. Guillory and C. E. Hunter, *J. Chem. Phys.* **50**, 3516 (1980).
30. V. E. Bondybey and L. E. Brus, *J. Chem. Phys.* **62**, 620 (1975); V. E. Bondybey and C. Fletcher, *J. Chem. Phys.* **64**, 3615 (1976); L. E. Brus and V. E. Bondybey, *J. Chem. Phys.* **65**, 71 (1976); V. E. Bondybey, S. S. Bearder and C. Fletcher, *J. Chem. Phys.* **64**, 5243 (1976); V. E. Bondybey and L. E. Brus, *Advan. Chem. Phys.* **41**, 269 (1980).
31. R. Schriever, M. Chergui and N. Schwentner, *J. Chem. Phys.* **95**, 6124 (1991).
32. H. Kunz, J. G. McCaffrey, R. Schriever and N. Schwentner, *J. Chem. Phys.* **94**, 1039 (1991).
33. *Handbook of Bimolecular and Termolecular Gas Reactions, Vol. III*, J. A. Kean, Ed., CRC Press, Boca Raton, FL (1987).
34. M. E. Fajardo and V. A. Apkarian, *J. Chem. Phys.* **89**, 4102 (1988).
35. A. I. Katz and V. A. Apkarian, *J. Phys. Chem.* **94**, 6671 (1990).

36. A. J. Barnes, H. E. Hallam and G. F. Scrimshaw, *Trans. Faraday Soc.* **65**, 3150 (1969); **65**, 3159 (1969); **65**, 3172 (1969).
37. D. F. Cowgill and R. E. Norberg, *Phys. Rev.* **B13**, 2773 (1976).
38. D. G. Williams and K. D. Bayes, *J. Am. Chem. Soc.* **90**, 1957 (1968).

Publications Supported by Contract F29609-91-C-0016

1. Photoproduction and Dynamics of Oxygen Atoms in Xenon Matrices, E. Todd Ryan and Eric Weitz, *J. Chem. Phys.* **99**, 1004 (1993).

2. Photodepletion and Dynamics of Oxygen Atoms in Xenon Matrices, E. Todd Ryan and Eric Weitz, *J. Chem. Phys.* **99**, 8628 (1993).

3. H Atom Mobilities in Xenon Matrices. Dependence on Matrix Morphology, D. LaBrake and Eric Weitz, *Chem. Phys. Lett.*, **211**, 430 (1993).

4. Vibrational Relaxation of HCl as a Function of Xenon Density: The Role of HCl−Xe Complexes, Antonis Moustakas and Eric Weitz, *J. Chem. Phys.*, **98**, 6947 (1993).

5. O Atom Photoproduction Dynamics and Reactions in Cryogenic Solids, E. Todd Ryan and Eric Weitz, *Chem. Phys.*, **188** (1994).

6. Photochemistry and Reaction Dynamics of HBr in Xenon Matrices: I. Photodissociation of HBr and Production of Br Atoms, D. LaBrake, E. T. Ryan and E. Weitz, to be published.

7. Photochemistry and Reaction Dynamics of HBr in Xenon Matrices: II. Photodissociation of HBr and Production of H Atoms, D. LaBrake, E. T. Ryan and E. Weitz, to be published.

8. The Effect of Deposition Temperature on the Mobility of Matrix Isolated Species: HBr in Xenon, D. H. Fairbrother, D. LaBrake and E. Weitz, to be published.